siam

15th Annual Meeting of the Bulgarian Section of SIAM
December 15-17, 2020
Sofia

BGSIAM'20

EXTENDED ABSTRACTS

HOSTED BY THE JOINT INNOVATION CENTRE
BULGARIAN ACADEMY OF SCIENCES

15th Annual Meeting of the Bulgarian Section of SIAM
December 15-17, 2020, Sofia

BGSIAM'20 Extended abstracts

ISSN: 1313-3357 (print)
ISSN: 1314-7145 (electronic)

Printed in Sofia, Bulgaria

PREFACE

The Bulgarian Section of SIAM (BGSIAM) was formed in 2007 with the purpose to promote and support the application of mathematics to science, engineering and technology in Republic of Bulgaria. The goals of BGSIAM follow the general goals of SIAM:

- To advance the application of mathematics and computational science to engineering, industry, science, and society;
- To promote research that will lead to effective new mathematical and computational methods and techniques for science, engineering, industry, and society;
- To provide media for the exchange of information and ideas among mathematicians, engineers, and scientists.

During BGSIAM'20 conference a wide range of problems concerning recent achievements in the field of industrial and applied mathematics will be presented and discussed. The meeting provides a forum for exchange of ideas between scientists, who develop and study mathematical methods and algorithms, and researchers, who apply them for solving real life problems.

The strongest research groups in Bulgaria in the field of industrial and applied mathematics, advanced computing, mathematical modelling and applications will be presented at the meeting according to the accepted extended abstracts. Many of the participants are young scientists and PhD students.

LIST OF INVITED SPEAKERS:

- Oleg Iliev (Fraunhofer Institute for Industrial Mathematics, Kaiserslautern, Germany)
  "Pore scale simulation of reactive flow for industrial and environmental problems"
- Geno Nikolov (Sofia University, "St. Kliment Ohridski", Bulgaria)
  "Markov type inequalities and extreme zeros of orthogonal polynomials "
- Michail Todorov (Technical University of Sofia, Bulgaria)
  "Vector Schrodinger equation: Nonlinearity, Multidimensionality, Integrability. What to Prefer?"

The present volume contains extended abstracts of the presentations (Part A) and list of participants (Part B).

Ivan Georgiev
Chair of BGSIAM Section

Hristo Kostadinov
Vice-Chair of BGSIAM Section

Elena Lilkova
Secretary of BGSIAM Section

Sofia, December 2020

Table of Contents

Part A

Extended abstracts[1]

[1] Arranged alphabetically according to the family name of the first author.

Sensitivity of the nonlinear matrix equation $X^p = A + M(B + X^{-1})^{-1}M^*$

Vera Angelova

In this paper, we consider the nonlinear matrix equation

$$F(X, Q) := X^p - A - M(B + X^{-1})^{-1}M^* = 0, \tag{1}$$

for a positive integer $p \geq 1$ and a collection of data $n \times n$ matrices $Q := (A, B, M)$, where A and B are Hermitian positive semidefinite matrices and M - an arbitrary matrix. For $p \geq 2$, when A and B are positive semidefinite matrices, equation (1) has a unique positive definite solution X. For the case $p = 1$, equation (1) is the well known in control theory, stochastic filtering, dynamic programming and ladder network symmetric discrete-time algebraic Riccati equation $X = MX(I+BX)^{-1}M^*+A$ and when $B = 0$, it becomes the Stein equation, arising in signal processing, system and control theory. The sensitivity and the conditioning of the symmetric discrete-time algebraic Riccati equation and the Stein equation have been studied and local and nonlocal perturbation bounds have been proposed in the literature, as well. We are interested in the sensitivity of the solution X to equation (1) to perturbations in the data. The sensitivity analysis of equation (1) intertwines the challenges of the properties of the symplectic Hamiltonian $f(X) = A + M(B + X^{-1})^{-1}M^*$ with those of the matrix power function $g(X) = X^p$.
In this paper, applying the local and the nonlocal perturbation analysis, based on the techniques of Fréchet derivatives, the method of Lyapunov majorants and Schauder fixed point principle, local and nonlocal perturbation bounds are derived. The local bounds are first order perturbation bounds for the error in the solution X to (1), formulated on the base of absolute and relative condition numbers of the equation and valid only asymptotically for sufficiently small perturbations in the data. Unfortunately the allowable size of the perturbations depends on the properties of the given problem and no one can a priori determine it in order to assure rigorism of the local bound. The nonlocal perturbation bound involves the local bound, as well as terms of second and higher order of the perturbations in the data included in a given a priori prescribed domain that guarantees the existence of an unique solution to the perturbed equation in a neighborhood of the unperturbed solution. This leads the disadvantages of the nonlocal bound to be more pessimistic than the local bound and to may not exist, when the condition of its existence is violated. Numerical examples illustrate the effectiveness of the perturbation bounds proposed.

Acknowledgments. This work is accomplished with the partial support by the Grant BG PLANTNET "Establishment of national information network genbank — Plant genetic resources".

Adjoint State Optimization Algorithm for Prediction of Honeybee Population Losses

Atanas Z. Atanasov, Slavi G. Georgiev

The first common record of a ubiquitous massive loss of honeybee colones date from the winter of 2006–2007. Some apiaries have lost about 90% of their colonies and this phenomenon is observed in USA, Europe and other destinations. There were another events concerning *honeybee losses* in the far and near history at different places, but in the early 2007, there were beekeepers who experienced $80-100\%$ losses. Such an extraordinary event, besides its environmental and economic impact, attracts a lot of scientific interest and is a topic of a vast body of research.

There are conditions described by the absence of adult bees, but particular losses in the winters of 2007, 2008 and other recent years share similar symptoms and the causal syndrome is called 'Colony Collapse Disorder' (CCD). It is characterized by three distinguishable traits: 1) a rapid loss of adult bees in colonies while no dead bodies are found in and around the hive; 2) the presence of the queen and the capped brood; 3) the presence of a food stores which, as well as the hive, are not robbed by pests or scavengers for an extended period of time.

The task of protecting bee colonies is becoming increasingly important for the world around us. Albert Einstein said that *mankind would survive four years after extinction of the bees. There are no crops without pollination; animals will die of hunger – and the people with them.*

Now we will describe a model of CCD in a honeybee colony. We follow the basic honeybee population model proposed by [1], rewritten as

$$\frac{\mathrm{d}N}{\mathrm{d}t} = L\frac{N}{\omega+N} - mF, \qquad \frac{\mathrm{d}F}{\mathrm{d}t} = \alpha N - (\alpha+\sigma+m)F + \sigma\frac{F^2}{N} \tag{2}$$

with initial condition $N(t_0) = N^0$, $F(t_0) = F^0$.

H is *the number of bees working in the hive* and F – *the number of bees who work outside the hive* hereafter referred to as *foragers*. All adult worker bees could be classified either as hive bees or as foragers, and that there is no overlap between these two behavioral classes, hence *the total number of adult worker bees in the colony* is $N = H + F$. We let $\boldsymbol{p} = (p^1, p^2, p^3, p^4)$, $p^1 := m$, $p^2 := \alpha$, $p^3 := \sigma$, $p^4 := \omega$, $\boldsymbol{p} \in \mathbb{S}_{\mathrm{adm}} = \left\{\boldsymbol{p} \in \mathbb{R}^4 :\ 0 < p^i < P^i,\ i = 1,2,3,4\right\}$.

Hereinafter all solutions $\{N(t;\boldsymbol{p}), F(t;\boldsymbol{p})\}$, $\boldsymbol{p} \in \mathbb{S}_{\mathrm{adm}}$ are defined on the interval $t_0 \le t \le T$. When the parameters m, α, σ and ω are known, the problem (2) is well-posed and it is called a *direct problem.*

We study the *inverse problem* of reconstructing the parameter $\boldsymbol{p} \in \mathbb{S}_{\mathrm{adm}}$ by means of the observed behaviour $N(t^k;\boldsymbol{p}) = Y_k,\ k = 1,\ldots,K_N,\ F(t^k;\boldsymbol{p}) = Z_k,\ k = 1,\ldots,F_N$ of the dynamical system (2). Then, the inverse problem of the parameter reconstruc-

tion can be formulated in a variational setting as follows:

$$\min_{\boldsymbol{p}\in \mathrm{S}_{\mathrm{adm}}} \Phi(\boldsymbol{p}), \quad \Phi(\boldsymbol{p}) = \Phi(m,\alpha,\sigma,\omega) = \Phi_N(\boldsymbol{p}) + \Phi_K(\boldsymbol{p}),$$
$$\Phi_N(\boldsymbol{p}) = \sum_{k=1}^{K_N} \left(N(t^k;\boldsymbol{p}) - Y_k\right)^2, \quad \Phi_F(\boldsymbol{p}) = \sum_{k=1}^{K_F} \left(F(t^k;\boldsymbol{p}) - Z_k\right)^2.$$

The formulated inverse problem is solved by an adjoint equation gradient method, see e. g [2]. Namely, we that the gradient $J' \equiv (J'_m, J'_\alpha, J'_\sigma, J'_\omega)$ is given by (3)

$$\begin{aligned} J'_m(\boldsymbol{p}) &= \int_0^T (\varphi_N + \varphi_F) F \mathrm{d}t, \quad J'_\alpha = \int_0^T \varphi_F F \mathrm{d}t, \\ J'_\sigma(\boldsymbol{p}) &= \int_0^T \left(F - \frac{F^2}{N}\right) \varphi_F \mathrm{d}t, \quad J'_\omega(\boldsymbol{p}) = L \int_0^T \frac{N\varphi_N}{(\omega+N)^2} \mathrm{d}t, \end{aligned} \tag{3}$$

where the functions φ_N, φ_F are the solution to the adjoint final value problem

$$\begin{aligned} \frac{\mathrm{d}\varphi_N}{\mathrm{d}t} &= \frac{\omega}{(\omega+N)^2}\varphi_N - \left(\alpha - \sigma\frac{F^2}{N^2}\right)\varphi_F + 2\sum_{k=1}^{K_N} \left(N(t;\boldsymbol{p}) - Y(t)\right) \delta(t-t^k), \\ \frac{\mathrm{d}\varphi_F}{\mathrm{d}t} &= m\varphi_N + \left(\alpha + \sigma + \omega - 2\sigma\frac{F}{N}\right)\varphi_F + 2\sum_{k=1}^{K_F} \left(F(t;\boldsymbol{p}) - Z(t)\right) \delta(t-t^k), \end{aligned}$$

where $\delta(\cdot)$ is the Dirac-delta function, and

$$\varphi_N(T) = 0, \quad \varphi_F(T) = 0.$$

The numerical analysis suggests the farmer the role of accelerated forager recruitment in employing hives during a colony collapse.

Acknowledgments. The study of the first author is supported by contract 2020-FNI-01, funded by the Research Fund of the University of Ruse. This research is supported by Bulgarian National Science Fund under Project KP-06-PN 46-7 "Design and research of fundamental technologies and methods for precision apiculture".

References

[1] Khoury, D.S., Myerscough, M.R., Barron, A.B.: A quantitative model of honey bee colony population dynamics. PLoS ONE **6**(4), e18491 (2011)

[2] Marchuk, G.I., Agoshkov, V.I., Shutyaev, V.P.: Adjoint Equations and Perturbation Algorithms in Nonlinear Problems. CRC Press, Boca Raton (1996)

ETCCDI Precipitation-based Climate Indices in the CMIP5 Future Climate Projections over Southeast Europe

Hristo Chervenkov and Kiril Slavov

Today there is overall consensus about the paramount importance of the problem of the climate change. It will impact markedly the ecosystems, all branches of the international economy, and the quality of life. In climate change research, scenarios describe plausible trajectories of climate conditions and other aspects of the future. Emissions scenarios are descriptions of potential future emissions to the atmosphere of substances that affect the Earth's radiation balance, such as greenhouse gases (GHG) and aerosols. Along with information on other related conditions such as land use and land cover, emissions scenarios provide inputs to climate models. Coupled atmosphere-ocean general circulation models (CAOGCMs) allow the simulated climate to adjust to changes in climate forcing, such as increasing GHG. The Coupled Model Intercomparison Project (CMIP) is a standard experimental protocol for studying the output of CAOGCMs. The main aim of the fifth phase of CMIP, CMIP5, is to study the climate and climate change in the past, present and future, using a set of simulations in various spatial and temporal scales. The CMIP5 experiment uses new emission scenarios called representative concentration pathways (RCP) to assess the interactions between the human activities on the one hand and the environment on the other hand, and their evolution. The RCPs are mitigation scenarios that assume policy actions will be taken to achieve certain emission targets. Four RCPs have been formulated: RCP2.6, RCP4.5, RCP6.0 and RCP8.5 which are named after the possible range of 'radiative forcing' values at the end of the 21st century, relative to pre-industrial values — +2.6, +4.5, +6.0 and +8.5Wm^{-2}.

In the recent decades many studies are dedicated on the climate projections over Europe and the Mediterranean basin. Despite the overall agreement for general reduction of the precipitation amount in the middle and at the end of the 21th century, there are still many differences in the magnitude of the expected changes, annual and seasonal variability and spatial distributions. Central and Eastern Europe is a region where precipitation changes remain still uncertain.

The main aim of the present study is to perform overall assessment of the precipitation climate over Southeast Europe via the projected changes of top 5 precipitation-based climate indices (CIs): Annual count of days when the daily precipitation amount (PA) is greater or equal than 10 mm, Maximum length of dry spell, Monthly maximum consecutive 5-day PA, Annual total PA greater than the 95th percentile, calculated over the reference period 1961–1990 and Annual total PA in wet days, which are noted R10MM, CDD, RX5DAY, R95p and PRCPTOT correspondingly. The CIs are computed from the output of selected CMIP5 CAOGCMs. The assessment, performed on annual basis, is continuation of sets of previous our works and is regional study.

Today there is overall consensus that the multi-model ensembles are an indispens-

able tool for future climate projection and the quantification of its uncertainty. The equally weighted multi-model mean (MMM) is most often used as a "best" estimate for variable averages, as evidenced by its ubiquity in the 5th Assessment Report of the Intergovernmental Panel on Climate Change. Although the number of the considered models in our study is only four, the ensemble MMM is plausible way for common estimation and thus it is shown on Fig. 1. The study confirms, first of all, the complexity of the expected precipitation-related changes. It is revealed general drying tendency toward the end of the 21st century, which is quantified with increase of the indicator consecutive dry days and reduction of the annual precipitation sum. This

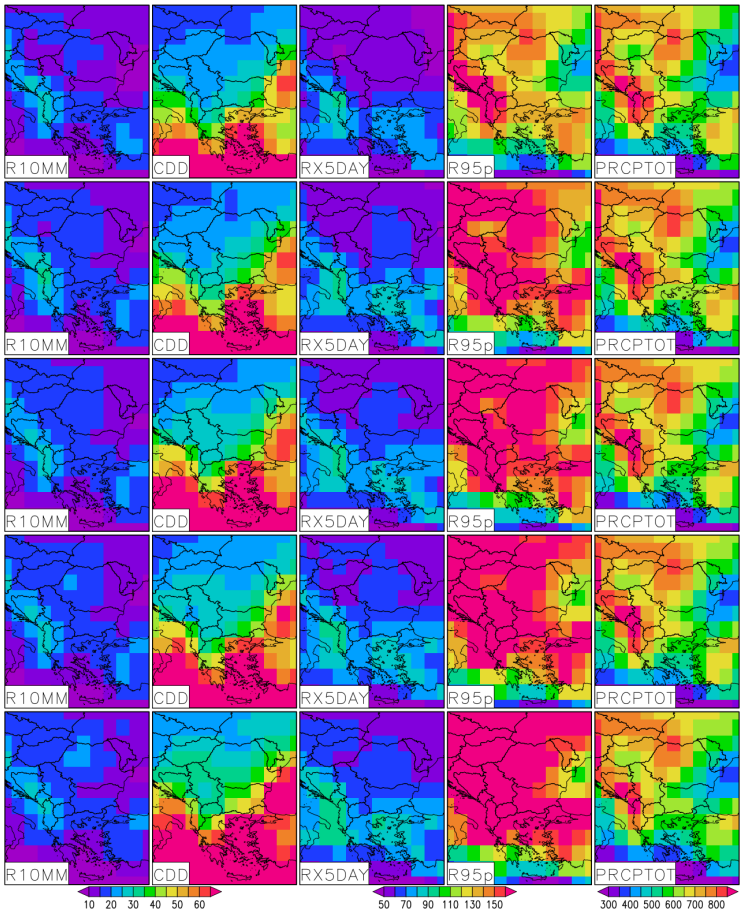

Figure 1: Ensemble MMM for the reference period on the first row; MMMs for RCP2.6, RCP4.5, RCP6.0 and RCP8.5 on the second, third, fourth and fifth row correspondingly. The units for R10MM and CDD are days; for RX5DAY, R95p and PRCPTOT - mm.

tendency, however, is accompanied by steady increases of the indicator very wet days. The last suggest that dry spells in the region, which are prerequisite for droughts, will become longer, but that precipitation may be more extreme when it occurs.
The results of this and similar studies could be methodologically reliable scientific basis of various impact studies and the development of adaptation strategies.

Stability Analysis of a Mathematical Model for Phenol and Cresol Mixture Degradation with Interaction Kinetics

Neli Dimitrova, Plamena Zlateva

Nowadays, organic chemical mixtures are among the most persistent environmental pollutants. Different aromatic compounds such as phenol, cresols, nitrophenols, benzene, etc. coexist as complex mixtures in wastewaters from petroleum refineries, coal mining and other industrial chemical sources. Biological degradation has recently become a viable green technology for remediation of organic pollutants in comparisson to other chemical and physical methods.

We propose a mathematical model for phenol and p-cresol mixture degradation in a continuously stirred bioreactor. The model is described by the following three nonlinear ordinary differential equations

$$\begin{aligned} \frac{dX(t)}{dt} &= (\mu(S_{ph}, S_{cr}) - D)\, X(t) \\ \frac{dS_{ph}(t)}{dt} &= -k_{ph}\, \mu(S_{ph}, S_{cr}) X(t) + D(S^0_{ph} - S_{ph}(t)) \\ \frac{dS_{cr}(t)}{dt} &= -k_{cr}\, \mu(S_{ph}, S_{cr}) X(t) + D(S^0_{cr} - S_{cr}(t)), \end{aligned} \tag{4}$$

where X is biomass concentration, S_{ph} is phenol concentration, S^0_{ph} is influent phenol concentration, S_{cr} is p-cresol concentration, S^0_{cr} is influent p-cresol concentration, D is dilution rate, and $\mu(S_{ph}, S_{cr})$ is the biomass specific growth rate, presented by

$$\mu(S_{ph}, S_{cr}) = \frac{\mu_{max(ph)} S_{ph}}{k_{s(ph)} + S_{ph} + \frac{S^2_{ph}}{k_{i(ph)}} + I_{cr/ph} S_{cr}} + \frac{\mu_{max(cr)} S_{cr}}{k_{s(cr)} + S_{cr} + \frac{S^2_{cr}}{k_{i(cr)}} + I_{ph/cr} S_{ph}}.$$

All coefficients in the model and in the expression of $\mu(\cdot)$ are assumed to be positive. The novel idea in the model design is the kinetic function $\mu(S_{ph}, S_{cr})$, known as *sum kinetics with interaction parameters* (SKIP) and involving inhibition effects. The interaction parameters $I_{cr/ph}$ and $I_{ph/cr}$ indicate the degree to which substrate p-cresol affects the biodegradation of substrate phenol, and substrate phenol affects the biodegradation of substrate p-cresol, respectively.

We determine the equilibrium points of the model and study their local asymptotic stability and bifurcations with respect to the practically important parameter D. It is shown that there exists values of D, $0 < D_1 < D_2 < D_3$, such that the following assertions are valid.

(a) The wash-out equilibrium $E_0 = (0, S^0_{ph}, S^0_{cr})$ (with $X = 0$) exists for all $D > 0$; E_0 is locally asymptotically unstable if $D \in (0, D_2)$, and E_0 is locally asymptotically stable if $D > D_2$.

(*b*) There are two interior (with positive components) equilibrium points,

$$E_1 = (X^{(1)}, S_{ph}^{(1)}, S_{cr}^{(1)}) \text{ and } E_2 = (X^{(2)}, S_{ph}^{(2)}, S_{cr}^{(2)}) \text{ with } S_{cr}^{(2)} > S_{cr}^{(1)},$$

such that E_1 exists for $D \in (D_1, D_3)$ and is locally asymptotically unstable, E_2 exists if $D \in (D_1, D_2)$ and is locally asymptotically stable.

(*c*) The interior equilibria E_1 and E_2 undergo a saddle-node bifurcation at $D = D_1$.

(*b*) The interior equilibrium E_2 and the wash-out equilibrium E_0 undergo a transcritical bifurcation at $D = D_2$.

The next theorem shows that the dynamic system (4) exhibits the standard properties that we would expect from a bioreactor model.

Theorem 1. Assume that $X(0) \geq 0$, $S_{ph}(0) \geq 0$, $S_{cr}(0)) \geq 0$ hold true.

(*i*) If $X(0) = 0$ then all model solutions tend to the equilibrium point $E_0 = (0, S_{ph}^0, S_{cr}^0)$.

(*ii*) If $X(0) > 0$ then $X(t) > 0$, $S_{ph}(t) > 0$, $S_{cr}(t) > 0$ for all $t > 0$.

(*iii*) All solutions are uniformly bounded for all $t \geq 0$ and thus exist for all $t \geq 0$.

We also establish the global stabilizability of the model dynamics towards the locally stable interior equilibrium point E_3 under some natural assumptions. The dynamic behavior of the solutions is demonstrated on numerical examples.

Acknowledgements. This study has been partially supported by the National Scientific Program "Information and Communication Technologies for a Single Digital Market in Science, Education and Security (ICTinSES)", contract No DO1–205/23.11.2018, financed by the Ministry of Education and Science in Bulgaria. The work of the first author has been partially supported by grant No BG05M2OP001-1.001-0003, financed by the Science and Education for Smart Growth Operational Program (2014–2020) in Bulgaria and co-financed by the European Union through the European Structural and Investment Funds.

Time series analysis of data from the fluid glazing experiment

Krasimir Geogriev, Nikolay K. Vitanov, M. Stoyanova

We study time series from the fluid glazing experiment performed in Sofia [1]. The time series are for different parameters of connected to the fluid flow in the experiment such as temperature, heat flow, etc. The analysis is made on the basis of the methodology of linear and nonlinear time series analysis [2] - [6]. We discuss the power spectra and autocorrelations connected with measured signals and apply the methodology of Principal Complonent Ananlys, Singular Values Decomposition and Time-Delay Phase Space Construction in order to extract additional information about the behavior of the fluid part of the experiment. The obtained results will form the basis for application of additional methodology from the arsenal of the nonlinear time series analysis and for simulation of the corresponding fluid flows.

References

[1] InDeWaG (Industrial Development of WaterFlow Glazing Systems) project *http* : *//www.indewag.eu*

[2] H. Kantz, T. Schreiber. Nonlinear Time Series Analysis, Cambridge University Press, Cambridge, 1997.

[3] P. J. Brockwell, R. A. Davis. Time Series: Theory and Methods, Springer, 1998.

[4] H. Kantz, D. Holstein, M. Ragwitz, N. K. Vitanov. Markov Chain Model for Turbulent Wind Speed Data. Physica A, **342**, 315 – 321 (2004).

[5] N. K. Vitanov, N. P. Hoffmann, B. Wernitz. Nonlinear Time Series Analysis of Vibration Data from a Friction Brake: SSA, PCA, and MFDFA. Chaos, Solitons & Fractals, **69**, 90 – 99 (2014).

[6] N. K. Vitanov, K. Sakai, Z. I. Dimitrova. SSA, PCA, TDPSC, ACFA: Useful Combination of Methods for Analysis of Short and Nonstationary Time Series. Chaos, Solitons & Fractals, **37**, 187 – 202 (2008).

Computational Homogenization for Determination of Elastic Material Properties of Closed Cell Foams

Ivan Georgiev, Roumen Iankov, Elena Kolosova, Michail Chebakov, Maria Datcheva

The foams are porous materials with open or closed cell structure. Metal foams, for example, are widely used in many industrial applications such as energy absorption structures, noise barrier structures, lightweight highly effective constructions and many other applications.
In the present paper, a 3D numerical homogenization strategy is proposed for determination of elastic material properties of closed cell foams. The performed homogenization procedure employs micro-computed tomography (micro-CT) and instrumented indentation testing data (IIT).
The results from the micro-CT testing are used to determinate the following characteristics of the considered foam material — the volume fractions of the pores and the solid phases, the average size of the pores, the pore size distribution in a representative volume element (RVE). Using the micro-CT data, a 3D geometrical model of the closed–cell foam's RVE is created and this geometrical model is used to generate the respective finite element model. For simplicity, the pores are considered to have a spherical form as it is depicted in Fig. 2. In order to apply the homogenization technique, in the finite element model of the closed–cell foam's RVE, the proper periodic boundary conditions are imposed. The obtained following the homogenization procedure six boundary value problems with periodic boundary conditions are solved using the finite element code ANSYS. The employed material model in the homogenization is the linear elastic model. The elastic properties of the solid phase are determined based on IIT data from testing of small volumes of the foam material. The determined elastic characteristics are analysed against data from literature in order to reveal the applicability of the followed in this study homogenization procedure.

Acknowledgement
The reported study was performed within the bilateral project funded by the Russian Foundation for Basic Research, research project No 19-58-18011 Bulg_a and by the Bulgarian National Science Fund, research project No KP-06-Russia-1. The first author gratefully acknowledges the financial support of the Bulgarian National Science Fund under Grant No. KP-06-H27-6. We also acknowledge the provided access to the infrastructure of the Laboratory for 3D Digitalization and Microstructure Analysis and of the Laboratory for Nanostructure Characterization, financially supported by the Science and Education for Smart Growth Operational Program (2014-2020) and the European Structural and Investment fund through Grant No BG05M2OP001-1.001-0003 and BG05M2OP001-1.001-0008.

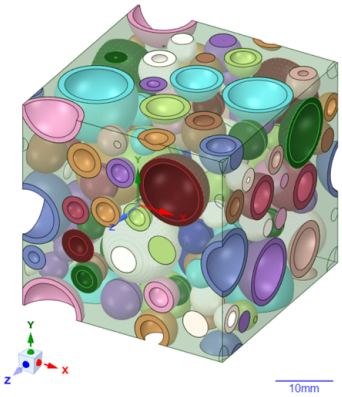

Figure 2: RVE with random particle distribution and spherical pores.

References

[1] Baltov, A., Iankov, R., Datcheva, M.: A New Approach to Determine the Yield Loci of Heterogeneous Media. J. Teor. Appl. Mech.. **4**, 13–19 (1996)

[2] ANSYS, Inc. Theory Reference Manual. Release 2019.

[3] Yang, Z. and Xiaofeng, P.: MicroCT scanning analysis for inner structure of porous media. Heat Trans. Asian Res., 36: 208-214 (2007)

Coefficient Identification for SEIR Model and Economic Forecasting in the Propagation of COVID–19

Slavi G. Georgiev, Lubin G. Vulkov

The COVID–19 pandemic is the global health crisis of the 21^{th} century. It was registered in humans in Wuhan, China by December 2019. This coronavirus causes a severe acute respiratory syndrome which could become potentially fatal. By the end of November 2020, there were more than 60 million confirmed cases of infected people and more than 1.4 million reported death cases globally.

The COVID–19 outbreak motivates the need to extend the application and development of different epidemic models. The coefficient identification of SIR epidemic models has seen recent success in providing a COVID–19 analysis [3]. In [1, 2], a time-dependent SEIR model is explored for mathematical and computer modeling of COVID–19 transmission dynamics in Bulgaria.

The Susceptible–Infected–Recovered (SIR) model is the most famous mathematical model for the spread of an infectious disease. Its formalism is the base of all current modeling of the dynamics and evolution infectious diseases, see e. g. [3]. The models are useful in understanding the basic principles of the COVID–19 [3].

Here, we work with the Susceptible–Exposed–Infected–Removed (SEIR) model

$$\frac{\mathrm{d}S}{\mathrm{d}t} = -\beta SI, \quad \frac{\mathrm{d}E}{\mathrm{d}t} = \beta SI - \alpha E, \quad \frac{\mathrm{d}I}{\mathrm{d}t} = \alpha E - \gamma I, \quad \frac{\mathrm{d}R}{\mathrm{d}t} = \gamma I. \tag{5}$$

We solve the system (5) at the initial conditions

$$S(0) = S_0,\ E(0) = E_0,\ I(0) = I_0, R(0) = R_0, \tag{6}$$

where S_0, E_0, I_0 and R_0 are non-negative constants. We will assume that the coefficients β, α are positive constants. Also, we assume that the infectious individuals leave the $I(t)$ class with rate γ and they move directly into the $R(t)$ class, removed population:

- Susceptible people $S(t)$, who are prone to contact the virus;
- Exposed population $E(t)$, who are infectious but asymptomatic;
- Infected individuals $I(t)$, which are currently sick;
- Removed people $R(t)$, who have already recovered or deceased from COVID–19.

Letting $\quad S(t) = e^{s(t)}, \quad I(t) = -\dfrac{1}{\beta}\dfrac{\mathrm{d}s}{\mathrm{d}t}(t), \quad R(t) = R_0 - \dfrac{\gamma}{\beta}(s(t) - s_0),$

$$E(t) = E_0 + I_0 + S_0 + R_0 - I(t) - S(t) - R(t),$$

the mathematical model (5),(6) is simplified in the form of a system of two ODEs:

$$\frac{\mathrm{d}s}{\mathrm{d}t} = -\beta I, \quad \frac{\mathrm{d}I}{\mathrm{d}t} = -(\alpha + \gamma)I - \alpha e^s + \frac{\alpha}{\beta}\gamma s - \frac{C_0}{\beta}, \quad 0 < t < T, \tag{7}$$

where $C_0 = \alpha\gamma \ln S_0 - \alpha\beta(S_0 + E_0 + I_0)$ with initial conditions $s(0) = s_0,\ I(0) = I_0$.

We will solve the *inverse problem* for determination of the unknown parameter vector $\boldsymbol{p} = (p^1, p^2, p^3) \equiv (\alpha, \beta, \gamma)$ at the measured values of the functions s, I:

$$s(t_k;\boldsymbol{p}) = Y_k,\ k = 1, \ldots, K_s, \quad I(t_k;\boldsymbol{p}) = Z_k,\ k = 1, \ldots, K_I.$$

The purpose of the inverse problem is to reconstruct these parameters from the observation data and based on that to evaluate the economic losses caused from COVID–19.
Very often, the point observation inverse problems are solved via the minimization of appropriate functionals. We will minimize the least-square functional

$$J(\boldsymbol{p}) = J(\alpha, \beta, \gamma) = J_s(\boldsymbol{p}) + J_I(\boldsymbol{p}) = \sum_{k=1}^{K_s} \left(s(t_k;\boldsymbol{p}) - Y_k\right)^2 + \sum_{k=1}^{K_I} \left(I(t_k;\boldsymbol{p}) - Z_k\right)^2.$$

The formulated inverse problem for (7) could be solved by gradient methods.
The gradient $J'_{\boldsymbol{p}} \equiv (J'_\alpha, J'_\beta, J'_\gamma)$ of the functional $J(\boldsymbol{p})$ is given by

$$J'_\alpha(\boldsymbol{p}) = \int_0^T \left(I + e^s - \frac{\gamma}{\beta} s\right) \varphi_I \mathrm{d}t,\ J'_\beta(\boldsymbol{p}) = \int_0^T \left(I\varphi_s + \frac{\alpha\gamma s - C_0}{\beta^2} \varphi_I\right) \mathrm{d}t,\ J'_\gamma(\boldsymbol{p}) = \int_0^T \left(I - \frac{\alpha}{\beta} s\right) \varphi_I \mathrm{d}t,$$

where the functions $\varphi_s = \varphi_s(t)$, $\varphi_I = \varphi_I(t)$ are the unique solutions to the *adjoint final-value problem*

$$\frac{\mathrm{d}\varphi_s}{\mathrm{d}t} = \left(\alpha e^s - \frac{\alpha\gamma}{\beta}\right) \varphi_I + 2 \sum_{k=1}^{K_s} \left(s(t;\boldsymbol{p}) - Y(t)\right) \delta(t - t_k),\ \varphi_s(T) = 0,$$
$$\frac{\mathrm{d}\varphi_I}{\mathrm{d}t} = \beta\varphi_s + (\alpha + \gamma)\varphi_I + 2 \sum_{k=1}^{K_I} \left(I(t;\boldsymbol{p}) - Z(t)\right) \delta(t - t_k),\ \varphi_I(T) = 0.$$

Computational experiments with synthetic and real demonstrate the capabilities of the numerical approach.
Acknowledgments. The authors are supported by the Bulgarian National Science Fund under Project DN 12/4 "Advanced analytical and numerical methods for nonlinear differential equations with applications in finance and environmental pollution", 2017.

References

[1] Kounchev O, Simeonov G, Kuncheva Z (2020) The TVBG-SEIR spline model for analysis of COVID–19 spread, and a tool for prediction scenarios. arXiv:2004.11338 [math.NA]

[2] Margenov S, Popivanov N, Ugrinova I, Harizanov S, Hristov Ts (2020) Mathematical and computer modeling of COVID-19 transmission dynamics in Bulgaria by time-dependent inverse SEIR model. arXiv:2008.10360 [q-bio.PE]

[3] Marinov TT, Marinova RS (2020) COVID–19 analysis using inverse problem for coefficient identification in SIR epidemic models. Chaos, Solitons & Fractals: X 100041

Recovering the Time-Dependent Volatility in European Options from Local and Nonlocal Price Measurements

Slavi G. Georgiev, Lubin G. Vulkov

Volatility is widely used in the risk management, portfolio hedging and option pricing, measuring the amount the randomness since volatility is the only unobservable parameter from the financial market, which, in general, could be estimated from the observed market option prices. So, the *calibration* of the volatility from observed market data seems to be of high interest, see e. g. [1]. What is more, both theoretical and empirical studies suggest that the volatility is far from constant but have strongly pronounced dependence on the remaining time to maturity, known as volatility term structure. An approximation of the time-dependent volatility $\sigma(\tau)$ we will seek by minimizing the objective functional

$$F(\sigma) = \int_0^T \left(C(S,\tau;\sigma) - C^\star(\tau)\right)^2, \tag{8}$$

where S is the price of the underlying asset, $C(S,\tau;\sigma)$ is the computed price and $C^\star(\tau)$ is the measured one.
We propose the following algorithm:

1. Specify an initial approximation $\sigma^{(0)}(\tau)$.
2. Assume that the approximate solution $\sigma^{(k)}(\tau)$ is known, and follow the steps to determine $\sigma^{(k+1)}(\tau)$.
3. Solve the direct problem Black–Scholes equation:

$$\frac{\partial C^{(k)}}{\partial \tau} - \frac{1}{2}\left(\sigma^{(k)}(\tau)\right)^2 \frac{\partial^2 C^{(k)}}{\partial S^2} - \left(r(\tau) - d(S,\tau)\right) S \frac{\partial C^{(k)}}{\partial S} + r(\tau) C^{(k)} = 0$$

   with the respective boundary conditions

$$\frac{\partial C^{(k)}}{\partial \tau}(0,\tau) + r(\tau) C^{(k)}(0,\tau) = 0$$

   and

$$C^{(k)}(S_{\max},\tau) = S_{\max} e^{-\int_0^\tau d(S_{\max},t)\mathrm{d}t} - K e^{-\int_0^\tau r(t)\mathrm{d}t}.$$

4. Solve the *adjoint* problem to the Black–Scholes equation:

$$\frac{\partial \varphi^{(k)}}{\partial \tau} = -\frac{1}{2}\left(\sigma^{(k)}(\tau)\right)^2 \frac{\partial^2 \varphi^{(k)}}{\partial S^2} - \left(r(\tau) - d(S,\tau)\right) S \frac{\partial \varphi^{(k)}}{\partial S} + r(\tau)\varphi^{(k)} - 2\left(\int_0^{S_{\max}} C_\tau^{(k)}(S,\tau)\mathrm{d}S - C^\star(\tau)\right)$$

   with terminal and boundary conditions

$$\varphi^{(k)}(S,T) = 0 \quad \text{and} \quad \varphi^{(k)}(0,\tau) = 0, \quad \varphi^{(k)}(S_{\max},\tau) = 0.$$

5. Determine the gradient of the functional F:

$$F'\left(\sigma^{(k)}(\tau)\right) = \int_0^{S_{\max}} C_\tau^{(k)}(S,\tau)\varphi^{(k)}(S,\tau)\mathrm{d}S.$$

6. Find $\sigma^{(k+1)}(\tau) = \sigma^{(k)}(\tau) - \alpha F'\left(\sigma^{(k)}(\tau)\right)$. Here α is a descent parameter which could be specified empirically.
7. To demonstrate the stability of the algorithm, perturbed data are introduced as follows:

$$C_\delta^\star(\tau) = C^\star(\tau)(1+\delta\xi),$$

where ξ is a random variable with a continuous distribution on the interval $[-1,1]$, $\delta > 0$ is the error tolerance.

Note that the proposed optimization algorithm could be also used if the initial information (8) is available only at some times τ_j, $j = 1,\ldots,K$:

$$\int_0^T C(S,\tau_j;\sigma)\mathrm{d}S = C^\star(\tau_j),\ j = 1,\ldots,K.$$

In this case, only the adjoint statement would change to

$$\frac{\partial\varphi^{(k)}}{\partial\tau} = -\frac{1}{2}\left(\sigma^{(k)}(\tau)\right)^2\frac{\partial^2\varphi^{(k)}}{\partial S^2} - \left(r(\tau) - d(S,\tau)\right)S\frac{\partial\varphi^{(k)}}{\partial S} + r(\tau)\varphi^{(k)} = 0, \quad \tau \neq \tau_j,$$
$$\left[\varphi^{(k)}\right]_{\tau=\tau_j} = -2\left(C^{(k)}(S,\tau_j) - C^\star(\tau_j)\right),\ S \in (0,S_{\max}), \quad j = 1,\ldots,K$$

with the same terminal and boundary conditions

$$\varphi^{(k)}(S,T) = 0 \quad \text{and} \quad \varphi^{(k)}(0,\tau) = 0, \quad \varphi^{(k)}(S_{\max},\tau) = 0.$$

In the same way we could process the 2D equation

$$\frac{\partial V}{\partial\tau} - \frac{1}{2}\sigma^2(\tau)\left(\sigma_1^2S_1^2\frac{\partial^2V}{\partial S_1^2} - 2\rho\sigma_1\sigma_2S_1S_2\frac{\partial^2V}{\partial S_1\partial S_2} + \sigma_2^2S_2^2\frac{\partial^2V}{\partial S_2^2}\right)$$
$$- \big(r(\tau) - d_1(S,\tau)\big)S_1\frac{\partial V}{\partial S_1} - \big(r(\tau) - d_2(S,\tau)\big)S_2\frac{\partial V}{\partial S_2} + r(\tau)V = 0.$$

The numerical experiments with synthetic and real data confirm that the proposed algorithm is capable of calculating the volatility level in an robust way.

Acknowledgments. The authors are supported by the Bulgarian National Science Fund under Project DN 12/4 "Advanced analytical and numerical methods for nonlinear differential equations with applications in finance and environmental pollution", 2017.

References

[1] Georgiev, S.G., Vulkov, L.G.: Computational recovery of time-dependent volatility from integral observations in option pricing. J. Comp. Sci. 39:101054 (2020)

[2] Marchuk, G.I., Agoshkov, V.I., Shutyaev, V.P.: Adjoint Equations and Perturbation Algorithms in Nonlinear Problems. CRC Press, Boca Raton (1996)

Numerical solvers based on weighted URA-averages

Stanislav Harizanov, Svetozar Margenov, Pencho Marinov

This talk is devoted to proposing and investigating efficient, yet numerically stable, numerical solvers for the algebraic problem

$$\mathbf{u} = (\mathbb{A}^{\alpha} + \mathbf{q}\mathbb{I})^{-\mathbf{1}}\,\mathbf{f},$$

where $\mathbb{A} \in \mathbb{R}^{N\times N}$ is a large-scale, sparse SPD matrix, $q \geq 0$, $\alpha \in (0,1)$, and $\mathbf{f} \in \mathbb{R}^{\mathbf{N}}$. For the matrix fractional power $\mathbb{A}^{\alpha}$ the spectral definition is used:

$$\mathbb{A}^{\alpha} = \mathbb{W}\mathbb{D}^{\alpha}\mathbb{W}^{T}, \qquad \mathbb{W} = [\mathbf{\Psi_1^T}, \mathbf{\Psi_2^T}, ..., \mathbf{\Psi_N^T}], \quad \mathbb{D} = \mathbf{diag}(\lambda_{\mathbf{1}}, \ldots, \lambda_{\mathbf{N}}),$$

where $\{(\lambda_i, \mathbf{\Psi_i})\}_{\mathbf{i=1}}^{\mathbf{N}}$ are the eigenvalues/eigenvectors of $\mathbb{A}$. Such a problem appears for example in finite element or finite difference discretization of fractional-in-space diffusion-reaction elliptic problems.

Unlike $\mathbb{A}$, the matrix $\mathbb{A}^{\alpha}$ is dense and it is impractical and even unrealistic (in terms of both computer memory and execution time) to explicitly use it. The alternative is to approximate the action of $(\mathbb{A}^{\alpha} + q\mathbb{I})^{-1}$ on $\mathbf{f}$ via a linear combination of positive diagonal shifts $(\mathbb{A} + d_i\mathbb{I})^{-1}$, $i = 1, \ldots, k$ of $\mathbb{A}$. Thus, one needs to solve k independent sparse linear systems instead of a dense one. In our previous works, it has been established that such a problem is related to univariate approximations of the function

$$g_q(z(t)) = g_q(t;\alpha) := \frac{z}{1+qz} = \frac{t^{\alpha}}{1+qt^{\alpha}}, \qquad t \in [\kappa(\mathbb{A})^{-1}, 1]$$

within the class of (k,k)-rational functions, i.e., of the form $P_k(t)/Q_k(t)$, with $P_k(t)$ and $Q_k(t)$ polynomials of degree k and $Q_k(t)$ is monic. By $\kappa(\mathbb{A}) = \lambda_N/\lambda_1$ we have denoted the condition number of the matrix. When no a priori knowledge on $\kappa(\mathbb{A})$ is given, it is theoretically best to approximate in the closed interval $t \in [0,1]$, and let us denote the corresponding element of best uniform approximation (BURA) by $r_q(t)$. For small α and large q the derivation of $r_q(t)$ is numerically instable process, especially when k increases. Therefore, based on the following identity, we have studied the URA alternatives $\bar{r}_{q_1,q_2}$, defined as

$$\frac{t^{\alpha}}{1+qt^{\alpha}} = \frac{\frac{t^{\alpha}}{1+q_1t^{\alpha}}}{1+q_2\frac{t^{\alpha}}{1+q_1t^{\alpha}}}, \quad q_1,q_2 \geq 0,\ q = q_1+q_2, \quad \Longrightarrow \quad \bar{r}_{q_1,q_2} := \frac{r_{q_1}(t)}{1+q_2r_{q_1}(t)}.$$

In this talk we further expand the family of potential approximants and consider weighted averages of two URA elements

$$\widetilde{r}_q := \omega_1\bar{r}_{q_1,q_2} + \omega_2\bar{r}_{q_1',q_2'}, \qquad \omega_1,\omega_2 \geq 0,\ \omega_1+\omega_2 = 1; \quad q_1+q_2 = q_1'+q_2' = q.$$

This leads to solving $2k$ sparse linear systems, instead of k, but the process is much more numerically stable and computationally reliable without increasing the order of the approximation error.

Acknowledgment: The partial support through the Bulgarian NSF Grant DN 12/1 is highly acknowledged.

Parallelizing multiple precision Taylor series method for integrating the Lorenz system

I. Hristov, R. Hristova, S. Dimova, P. Armyanov, N. Shegunov, I. Puzynin, T. Puzynina, Z. Sharipov, Z. Tukhliev

Computing mathematically reliable long-term trajectories of a chaotic dynamical system is not a trivial task due to the sensitive dependence on the initial conditions. However, the advances in numerical methods and computer technologies in recent years allow us to overcome these difficulties and give us new opportunities to explore the chaos. A key work in this direction is the paper of Shijun Liao [1]. He considers a new numerical procedure called "Clean Numerical Simulation" (CNS) to obtain verified numerical solutions of chaotic dynamical systems. The procedure is based on the multiple precision Taylor series method. A hybrid MPI+OpenMP strategy for parallelizing multiple precision Taylor series method, which implements CNS, is proposed, realized and tested. To parallelize the algorithm we combine MPI and OpenMP parallel technologies together with GMP library (GNU miltiple precision libary) and the tiny MPIGMP library. The details of the parallelization are explained on the paradigmatic model of the Lorenz system. We succeed to compute a reliable trajectory for the Lorenz attractor in the rather long time interval - [0,7000]. The solution was verified by comparing the results for 2700-th order Taylor series method and precision $\sim$ 3374 decimal digits and those with 2800-th order and precision $\sim$ 3510 decimal digits. With 192 CPU cores the 2800-th order computation lasted $\sim$ 145 hours with speedup $\sim$ 105.

References

[1] Liao, Shijun. "On the reliability of computed chaotic solutions of non-linear differential equations." Tellus A: Dynamic Meteorology and Oceanography 61.4 (2008): 550-564

Pore scale simulation of reactive flow for industrial and environmental problems

Oleg Iliev, Torben Prill, Pavel Toktaliev, Pavel Gavrilenko, Robert Greiner, Martin Votsmeier

Reactive flows in porous media are important processes in many industrial and environmental applications. The reactive transport in porous media is influenced by the pore scale interplay between convection, diffusion and reaction, coupled with the heterogeneity of the pore space (e.g., pore size distribution and connectivity) and chemical heterogeneity.

A 3D pore-scale mathematical model describes convection and diffusion in the pores together with heterogeneous (surface) or homogeneous (volumetric) reactions. Some media can be considered as two scale (micro scale and macro scale) ones, where the size of the resolved pores defines the micro scale, and the size of the porous domain as effective (averaged, homogenized) media defines the macro scale. Example are functionalized materials (e.g., those used in water purification). Other media can be considers as three scale ones. In addition to the two scales defined above, one considers also nano scale. Examples are, e.g., catalytic filters, air and water filters exploiting granulated active carbon particles, etc. In this case the catalyst (washcoat) particles and the active carbon particles are nano porous. Resolving simultaneously all three scales is not feasible on the existing computers, therefore a common approach is to build computational domains with resolved microscale pores, and to consider the nanoporous materials as effective (averaged) porous media.
To perform the pore-scale simulations for the above described problems, Fraunhofer ITWM has developed PoreChem, [1, 2], a software package dedicated to the simulation of reactive flow in the case of heterogeneous or homogeneous reactions. It enables the simulation of reactive flows in resolved porous media in a reasonable time. The software can compute the flow of a fluid in the pore space, as well as the diffusive and advective transport of solute species. The flow is computed by solving the Navier-Stokes-Brinkman system of equations with a finite volume discretization on a regular voxel grid. The geometries are usually coming from CT imaging technique, virtually generated images are also considered. The reactive transport is simulated by solving the reaction-diffusion-advection equation using the same space discretization. Different reaction kinetics, parametrized by reaction isotherms can be taken into account. The fast voxel based solver enables calculations directly on μCT-Images. Transient phenomena can be simulated, as well as steady state ones.
Pore scale simulations for two industrial problems will be presentated in this talk. Most attention will be paid on simulation for catalytic filters (in particular, diesel pariculate filter, DPF) [3]. The computational domain comes from a CT image of a piece of a manufactured filter. The role of the pore connectivity (manifested in channeling effects) and of the chemical heterogeneity (caused by the non-uniform distribution of the washcoat particles) will be discussed in details. Simulations with a generated, more homogeneous image, will also be presented. Further on, simulations for surface activated nonwoven filtering material will be also demonstrated.
Finally, some conclusions will be drawn, open questions will be formulated, and the forthcoming developments will be shortly announced.

References

[1] Calo, Victor M., Oleg Iliev, Z. Lakdawala, K. H. L. Leonard, and Galina Printsypar. "Pore-scale modeling and simulation of flow, transport, and adsorptive or osmotic effects in membranes: The influence of membrane microstructure." International journal of advances in engineering sciences and applied mathematics 7, no. 1-2 (2015): 2-13.

[2] Iliev, Oleg, Zahra Lakdawala, Katherine HL Neßler, Torben Prill, Yavor Vutov, Yongfei Yang, and Jun Yao. "On the pore-scale modeling and simulation of reactive transport in 3D geometries." Mathematical Modelling and Analysis 22, no. 5 (2017): 671-694.

[3] Greiner, Robert, Torben Prill, Oleg Iliev, Barry AAL van Setten, and Martin Votsmeier. "Tomography based simulation of reactive flow at the micro-scale: Particulate filters with wall integrated catalyst." Chemical Engineering Journal 378 (2019): 121919.

Suggesting a new approach for management of the cytokine storm using computer modeling and simulations

N. Ilieva, P. Petkov, M. Rangelov, N. Todorova, E. Lilkova, and L. Litov

Cytokine storm [1] is a state of overreaction of the innate immune system, characterised by a release of excessive amounts of pro-inflammatory cytokines. This condition can be triggered by a number of viral and bacterial infections, among them the ones caused by certain influenza strains and corona viruses, but is also associated with some autoimmune diseases. In the ongoing COVID-19 pandemic the cytokine storm, being the reason for acute respiratory distress syndrom (ARDS), accounts for about 70% of the deaths [2]. Thus, in order to devise therapeutic strategies to counteract SARS-CoV-2 infection it is crucial to develop a comprehensive understanding of how the virus hijacks the host and inactivates its immune response at the initial stage, how this relates to the delayed (over)reaction of the immune system and how this overreaction can be tamed. This knowledge is indispensable for developing new drugs, alongside with repurposing existing ones.

The two most important cytokines in the development of the cytokine storm are interleukin 6 (IL-6) and interferon-gamma (IFNγ). The former is involved in the regulation of B- and T-cells and the latter plays a key role in formation and modulation of the adaptive and innate immune response, though its over-expression is related to some autoimmune diseases (multiple sclerosis, myasthenia gravis, autoimmune uveitis etc.).

By means of molecular modelling and computer simulations we investigate the inhibitory action on the activity of IL-6 and IFNγ of fractionated heparin (low-molecular-weight heparin, LMWH). We show that LMWH oligosaccharides bind to IFNγ with high affinity at positions preventing cytokine's binding to its extracellular receptor (Fig. 3) and that way – the initiation of the IFNγ signalling pathway [3].

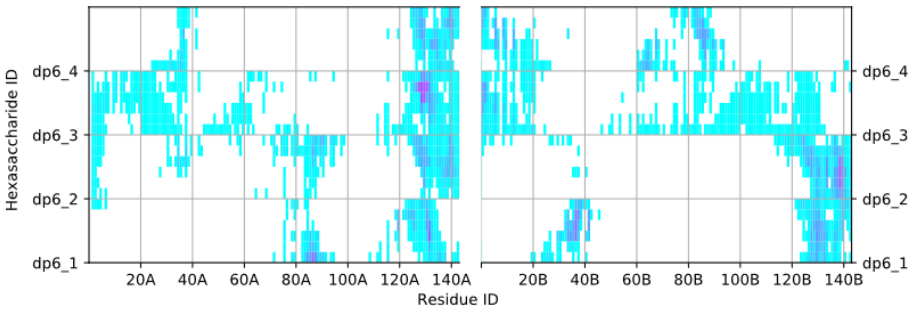

Figure 3: Pairwise contacts within 0.6 nm between IFNγ and the four LMWH molecules.

LMWH also engages with IL-6, forming a stable complex (Fig. 4) and blocking the bind-

ing sites required for the formation of the essential biologically active complex IL-6/IL-6Rα/gp130.

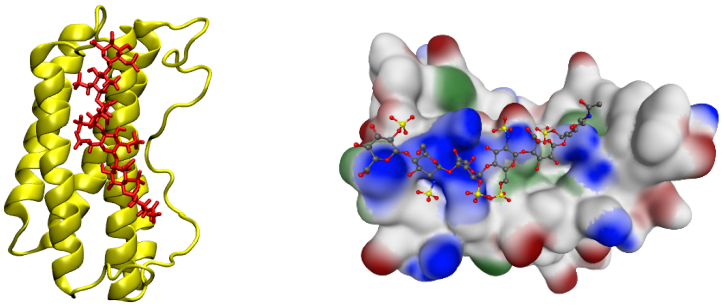

Figure 4: The complex between IL-6 and the LMWH molecule in two representations: IL-6 depicted in yellow, heparin in red (left panel); SAS representation of IL-6 with the standard colour coding, heparin coloured by atom type (right panel).

Our results reveal the inhibitory potential of LMWH oligosaccharides on key molecules in the development of the cytokine storm – IL-6 and IFNγ – and encourage further investigations on their applicability as an anti-inflammatory agent in the therapy and prevention of this potentially life-threatening condition.

Acknowledgements This work is partially supported by the Bulgarian Ministry of Education and Science (contract D01–205/23.11.2018) under the National Research Program "Information and Communication Technologies for a Single Digital Market in Science, Education and Security (ICTinSES)", approved by DCM # 577/17.08.2018. Computational resources were provided by the BioSim HPC Cluster at the Faculty of Physics at Sofia University "St. Kl. Ohridski" and the Centre for Advanced Computing and Data Processing, with the financial support by the Grant NoBG05M2OP001-1.001-0003, financed by the Science and Education for Smart Growth Operational Program (2014-2020) and co-financed by the European Union through the European structural and Investment funds.

References

[1] Clark, I.A. The advent of the cytokine storm. Immunology & Cell Biology. **85**(4) (2007) 271–273; doi.org/10.1038/sj.icb.710006

[2] Hojyo, S., Uchida, M., Tanaka, K., Hasebe, R., Tanaka, Y., Murakami, M., Hirano, T. How COVID-19 induces cytokine storm with high mortality. Inflammation and Regeneration. **40** (2020) doi.org/10.1186/s41232-020-00146-3

[3] Lilkova, E., Ilieva, N., Petkov, P., Rangelov, M. and Litov, L. *In Silico* Indications for Human Interferon Gamma Inhibition by Heparin. AIP Conf. Proc. **2302** (2020) 020003 doi.org/10.1063/5.0033537

Stationary flow of a substance in a channel with two branches

Tsvetelina I. Ivanova, Nikolay K. Vitanov

A mathematical model that describes the flow of a substance in a part of a network consisting of nodes that form a channel with two branches is formulated. It is based on difference equations which are studied in the stationary regime of motion of the substance: motion along the nodes of the network is present, but the quantity of substance in each cell remains constant over time. A class of probability distributions of the quantities of substance along the nodes of the network is obtained. Different cases of this class depending on the values of the model parameters are illustrated, including distributions along a single channel with periodic model coefficients.

References

[1] Vitanov, N. K., Vitanov, K. N. (2019). Statistical distributions connected to motion of substance in a channel of a network. Physica A: Statistical Mechanics and its Applications, 527, 121174.

[2] Vitanov, N. K., Vitanov, K. N. (2018). Discrete-time model for a motion of substance in a channel of a network with application to channels of human migration. Physica A: Statistical Mechanics and its Applications, 509, 635-650.

[3] Vitanov, N. K., Vitanov, K. N. (2018). On the motion of substance in a channel of a network and human migration. Physica A: Statistical Mechanics and its Applications, 490, 1277-1294.

[4] Vitanov, N. K., Vitanov, K. N. (2016). Box model of migration channels. Mathematical Social Sciences, 80, 108-114.

Numerical Determination of Reaction Coefficient in a Degenerate Stationary Problem of Air Pollution

Juri D. Kandilarov, Lubin G. Vulkov

The study of the dispersion of pollutants in the atmosphere is of extreme importance, because of the large number of industrial facilities and the effects of their emissions on the health of populations living in affected areas [3].

In this paper, we examine the estimation of reaction parameters appearing in stationary model for atmospheric flows, by using concentration measurements of tracer by a known source. The problem is assumed to be two-dimensional and is formulated by an advection-diffusion equation with a degenerate diffusion coefficient for the dispersion of the tracer in the atmosphere. It originates from the Monin-Obukhov atmosphere theory [3].

Direct problem. Our primary motivation comes from the two-dimensional stationary advection-diffusion equation

$$u\frac{\partial c}{\partial x}+(w-w_g)\frac{\partial c}{\partial z}-a\frac{\partial^2 c}{\partial x^2}-\frac{\partial}{\partial z}\left(b\frac{\partial c}{\partial z}\right)+k(x,z)c=f(x,z), \tag{9}$$

$(x,z)\in(0,X)\times(0,Z)$. The transport of air-borne pollutant in the atmosphere (and in water) at some simplification can be described by this equation [2, 3] where c is the *concentration of pollutants*, (u,w) are the components of the wind velocity, $w_g=const.>0$ is the falling velocity of the pollutants by gravity, f is the power of source, $k(x,z)$ is the transformation coefficient of the pollutants and a,b are the horizontal and vertical diffusion coefficients.

For the transversal eddy-diffusivity the expression is often used

$$b(z,t)=z(Z-z)\left(1-22\frac{z}{L}\right), \tag{10}$$

where $L<0$ is the Monin-Obukhov length, see e.g. [3]. To solve numerically the direct problem due to the degeneracy we use the method of Song Wang [4].

Inverse problem. For the inverse problem of interest here, the function $k(x,z)$ is regarded as unknown. Such function will be estimated by using measurements of the concentration $c(x,z)$ taken at the locations (x_i,z_i), $i=1,...,I$

$$c(x_i,z_i)=c_i^*,\quad (x_i,z_i)\in D,\quad i=1,...,I \tag{11}$$

As in the most applications, we reformulate the inverse problem (9)-(11) in the form of minimization of the square error functional

$$J(k(x,z))=\frac{1}{2}\sum_{i=1}^{I}(c(x_i,z_i)-c_i^*)^2 \tag{12}$$

The conjugate gradient method, with an adjoint problem is used for the minimization of the objective functional. Such minimization procedure requires the solution of auxiliary problems, known as sensitivity and adjoint problems, see [1]:

$$u\frac{\partial \triangle c}{\partial x}+(w-w_g)\frac{\partial \Delta c}{\partial z}-a\frac{\partial^2 \Delta c}{\partial x^2}-\frac{\partial}{\partial z}\left(b\frac{\partial \Delta c}{\partial z}\right)+k(x,z)\Delta c+\Delta k c=0, \tag{13}$$

$$J_\lambda[k(x,z)] = \frac{1}{2}\iint_D \sum_{i=1}^{I}(c(x_i,z_i;k)-c_i^*)^2\delta(x-x_i,z-z_i)dxdz \tag{14}$$
$$+\iint_D \left[u\frac{\partial c}{\partial x}+(w-w_g)\frac{\partial c}{\partial z}-a\frac{\partial^2 c}{\partial x^2}-\frac{\partial}{\partial z}\left(b\frac{\partial c}{\partial z}\right)+k(x,z)c-f(x,z)\right]\lambda(x,z)dxdz,$$

where $\delta(.)$ is the Dirac-delta function. The adjoint problem for the Lagrangian multiplier λ is

$$-u\frac{\partial \lambda}{\partial x}-(w-w_g)\frac{\partial \lambda}{\partial z}-a\frac{\partial^2 \lambda}{\partial x^2}-\frac{\partial}{\partial z}\left(b\frac{\partial c}{\partial z}\right)+k(x,z)\lambda=-\sum_{i=1}^{I}(c(x_i,z_i;k)-c_i^*)^2 \tag{15}$$

Now we find the gradient of $J_\lambda[k]$ with respect to $k(x,z)$:

$$\nabla J[k(x,z)] = \lambda(x,z)c(x,z). \tag{16}$$

The iterative procedure of conjugate gradient method is written as follows:

$$k^{s+1}(x,z) = k^s(x,z)-\alpha^s d^s(x,z), \quad s=0,1,..., \tag{17}$$

where $d^s(x,z)$ is the direction of descent, α is the search step size, and s is the number of iterations:

$$d^0(x,z)=\nabla J[k(x,z)],\ \ d^s(x,z)=\nabla J^s[k(x,z)]+\beta^s\nabla J^{s-1}[k(x,z)], \quad s=1,2,...\ , \tag{18}$$

where β^s is the conjugation coefficient:

$$\beta^0=0,\ \ \beta^s=\frac{\iint_D J^s[k(x,z)]^2dxdz}{\iint_D J^{s-1}[k(x,z)]^2dxdz}, \quad s=1,2,...\ . \tag{19}$$

$$\alpha^s=\frac{\sum_{i=1}^{I}(c(x_i,z_i)-c_i^*)\Delta c^s[c^s(x^i,z^i)]}{\sum_{i=1}^{I}(\Delta c^s(x_i,z_i))^2} \tag{20}$$

where $c^s(x_i,z_i)$ and $\Delta c^s(x_i,z_i)$ are the solutions of the direct and the inverse problems, respectively, at s-th iteration obtained by setting $k(x,z)=k^s(x,z)$ and $\Delta k(x,z)=\Delta^s(x,z)=d^s(x,z)$.
Then the computational algorithm in eight steps is obtained.

References

[1] O. M. Alifanov, E. A. Artyukhin, S. V. Rumyantsev Extreme Methods for Solving Ill-Posed Problems with Applications to Inverse Heat Transfer Problems, Begell House, New York - Wallingford (U.K.) (2015)

[2] Q. A. Dang and N. V. Luoc, Numerical solution of a stationary problem of air pollution, Proc. of NCST of Vietnam 6 (1994) 11-23.

[3] J. M. Stokie, SIAM, Review, **53**(2), 349-372 (2011).

[4] S. Wang, IMA J. of Numer. Anal., **24**, 699-720 (2004).

Fast Positivity Preserving Numerical Method for Time-Fractional Regime-Switching Option Pricing Problem

Miglena Koleva, Lubin Vulkov

We consider the following backward ($t \to T - t$) regime-switching problem [5]

$$\frac{\partial^\alpha V^k}{\partial t^\alpha} = L^k(V) - \sum_{\substack{j=1 \\ k \neq j}}^{m} \lambda_{kj}(V^k - V^j), \quad S \geq 0, \quad t \in (0,T], \quad k = 1,2,\ldots,m, \tag{21}$$

$$L^k(V) := \frac{1}{2}\left(\sigma^k(t,S)S\right)^2 \frac{\partial^2 V^k}{\partial S^2} + r^k S \frac{\partial V^k}{\partial S} - r^k V^k,$$

$$V^k(t,S) = V_r^k(t) \geq 0, \quad S \to \infty, \quad t \in (0,T], \tag{22}$$

$$V^k(0,S) = V_o(S) \geq 0, \quad S \geq 0, \tag{23}$$

where $\frac{\partial^\alpha V^k}{\partial t^\alpha}$ is the Caputo fractional derivative of order $0 < \alpha < 1$ and $\Gamma(\cdot)$ is Gamma function. The unknown solution $V^k(t,S)$ in (21)- (23) is the value of European option at time $0 \leq t \leq T$ for underlying asset $S \geq 0$ in regime k for a given payoff $V_o(S)$ at the expiry date T, r^k and σ^k, $k = 1,2,\ldots,m$ are set of discrete risk-free interest rates and and volatilities, respectively.

In the case of one regime ($m = 1$) and $\alpha = 1$, we obtain classical Black-Scholes equation. While, if we consider $m = 1$ and $0 < \alpha < 1$ the problem (21)- (23) is time-fractional Black-Scholes equation. If $m > 1$ and $\alpha = 1$, we derive regime-switching option pricing models.

Regime-switching models, $\alpha = 1$ are one of the extensions of the classical Black-Scholes equation to adopt more realistic description for asset price dynamics [2]. Such models are widely investigated in the literature.

Recently, with discovery of the fractional structure of financial market, in order to extend the financial theory, the fractional Black-Scholes equations are considered by many authors [1, 3].

In contrast, the results for fractional order option pricing regime-switching models are scare in the literature.

Numerical method for regime-switching model involving tempered fractional order partial derivatives governing the price of American options whose underlying asset follows a geometry Lévy process is developed in [4].

The Caputo time-fractional PDE when the dynamic of underlying asset price follows a regime-switching model in which the risky underlying asset depends on a continuous-time hidden Markov chain process is considered in [5]. Authors construct exact solution for particular cases of one and two regimes using the invariant subspace method.

In this paper, we consider a more general model [5] for which the closed form solution is not derived. Therefore, we construct numerical method. To the best of our knowledge there are no numerical results for such model in the literature.

The main difficulties of the model can be summarized as follows. From the properties of the Caputo derivative, the time-fractional system has a natural weak singularity at $t = 0$ [6], also the Black-Scholes operator degenerates at $S = 0$ and the initial function is not smooth.

Another complication in the numerical solving the model problem is in the treatment of the memory integral arising from the discretization of Caputo time derivative. The solution process involves, at any given time step, the history of all computed solutions at each previous time levels. Therefore, we need to store and operate on the entire history of the numerical solution.
On the present work we establish maximum principle for the differential problem (21)- (23), $0 < \alpha < 1$, $m > 1$. Then, we construct positivity preserving fast numerical method for solving the time-fractional regime-switching model problem. To accelerate the computational efficiency we develop two-grid method, based on iteration method for solving the linear system of algebraic equations. Using the two-grid method we separate the coupled problem into single subproblems. To cope with singularity and non-smooth effect of the payoff we use graded mesh in time and adapted mesh in space.

This work is supported by the Bulgarian National Science Fund under Project DN 12/4 "Advanced analytical and numerical methods for nonlinear differential equations with applications in finance and environmental pollution", 2017.

References

[1] Zhongdi Cen, Jian Huang, Aimin Xu, Anbo Le: Numerical approximation of a time-fractional Black-Scholes equation, Computers & Mathematics with Applications 75(8), 2874–2887 (2018).

[2] Elliott, R. J., Chan L. L., Siu, T. K., Option pricing and Esscher transform under regime switching, Ann. Finance 1(4), 423–432 (2005).

[3] Koleva, M., Vulkov, L.: Numerical solution of time-fractional Black-Scholes equation, Comp. Appl. Math. **36**(4), 1699–1715 (2017).

[4] Lei, S.-L., Wang, W., Chen, X.: A fast preconditioned penalty method for American options pricing under regime-switching tempered fractional diffusion models, J. Sci. Comput. 75, 1633–1655 (2018).

[5] Saberi, E, Hejazi. R., Dastranj, E.: A new method for option pricing via time-fractional PDE, Asian-European Journal of Mathematics 11(5), 1850074 (2018).

[6] Stynes, M., O'Riordan, E., Gracia, J.L.: Error analysis of a finite difference method on graded meshes for a time-fractional diffusion equation, SIAM J. Numer. Anal. 55 (2), 1057–1079 (2017).

Some problems of one-dimensional non-stationary linear-viscoelastic wave propagation

Korovaytseva E.A., Pshenichnov S.G., Zhelyazov T., Datcheva M.

Materials exhibiting hereditary properties are widely used in construction, aerospace industry, mechanical engineering, and are also objects of study in geophysics, seismology, biology, medicine and other fields. During exploitation, or in emergency situations, structures made of such materials can be subjected to various kinds of dynamic effects, including non-stationary ones. One of the important directions in the study of wave processes in viscoelastic bodies is analytical study based on the construction of solutions for initial and boundary value problems in linear viscoelasticity. Such studies have more than value in themselves and their results can be used for verification for numerical methods, be an integral part of complex computational procedures, and also be used in planning experiments and solving problems related to dynamic stability, destruction, optimization, etc.

In the past few decades, works of a number of authors have been devoted to the construction of solutions of linear viscoelastic dynamic problems and to the study of transient wave processes in viscoelastic materials and structures. Let us highlight some basic research approaches in this area. One of them uses the extension of Voltaire's principle to linear viscoelastic dynamic problems. However, due to the great mathematical difficulties, the class of the studied problems employing this approach is significantly limited in terms of imposed conditions on the properties of the material. Another approach to solve viscoelastic dynamic problems involves a special kind of integral convolution of the solution of the corresponding elastic dynamic problem with the solution of some auxiliary one-dimensional dynamic problem in which the hereditary kernels of the linear-viscoelastic material participate. One of the most common procedures for constructing solutions of non-stationary dynamic problems in linear viscoelasticity is the application of the Laplace transform with consequent inversion. Due to the complexity of the inversion operation, it is often performed asymptotically and therefore over a limited range of time or with significant restrictions on the material properties. A numerical-analytical method is known which lies in expanding the solution of the non-stationary viscoelasticity problem in a series in terms of eigenmodes of free vibrations of the corresponding elastic body (modal expansion method). However, its effectiveness is significantly reduced when Poisson's ratio is not constant. There is an approach in which the solution of the initial and boundary value problem is represented in a form of spectral expansions in biorthogonal systems of eigenfunctions of mutually conjugate pencils of differential operators. In the past few years, attention has been paid to the study of dynamics of thin-walled viscoelastic structures, including those in shock interaction, within the framework of models with fractional derivatives and other fractional-order operators. In this case, algebra of operators of fractional order is used, as well as the ray method. Methods for studying dynamic problems in viscoelasticity for auxetic materials, i.e. materials with negative Poisson's ratio, are also developed.

However, despite advances in the study of transient wave processes in viscoelastic media by analytical methods, many questions remain unresolved. Even for one-dimensional non-stationary dynamic problems, the results in some cases were obtained in a limited time range, or at low viscosity. In other cases, a number of significant restrictions are imposed on hereditary kernels, which greatly narrows the field of applicability of the results. Sometimes

decisions are presented in a form that is difficult to analyze. It is not sufficiently studied how the transition process is affected by the belonging of viscoelastic kernels to one or another class of functions and which parameters of the kernels are most clearly manifested in this case.

The aim of this work is to construct solutions of dynamic problems concerning one-dimensional transient wave processes in a homogeneous layer and in a homogeneous cylinder with a coaxial rigid inclusion. And also, to study, based on the constructed solutions, the processes of wave propagation in the considered constructions with specific initial data.

We consider an infinite layer with two plane-parallel boundary surfaces. One of the surfaces of the layer is rigidly embedded, and the other, starting from a certain moment, is subjected to the influence of a dynamic external load, evenly distributed over this surface. On the other hand, the considered cylinder is of an infinite length and contains a coaxial cylindrical rigid inclusion. Moreover, its outer surface is exposed to either normal or tangential dynamic load, evenly distributed over the surface.

For the considered initial and boundary value problems, the Laplace transform is applied and the solutions are found in transforms. Some general properties of the Laplace transforms in problems of this kind were investigated in earlier works by one of the authors (S.G. Pshenichnov). These properties made it possible to effectively apply the methods of contour integration and present the solutions in originals either in the form of series in residues at the poles of the images, or in a form containing an integral along the positive part of the imaginary axis. Some special cases are considered when the solution is signifficantly simplified.

The constructed in the present work solutions made it possible to study transient wave processes in a wide range of variation in the initial data. Based on the corresponding solutions for the cylinder with rigid inclusion it is revealed the dependence of maximum dynamic stress concentration at the boundary of the rigid inclusion on the ratio of the inclusion radius to the cylinder radius.

The presented results are showing the influence of the parameters of the hereditary kernels of the material on the nature of transient wave processes. It is demonstrated how hereditary kernels of different types (singular or regular), under appropriate conditions, can influence the wave processes in a similar way.

Acknowledgments: The reported study was performed within the bilateral project funded by the Russian Foundation for Basic Research (RFBR), project number 20-58-18002 and by the Bulgarian National Science Fund, project number KP-06-PRUSSIA-136.

Curve Fitting Motivated Differential Evolution Mutation

Georgi Kostadinov, Petar Tomov, Iliyan Zankinski

Introduction

Differential Evolution is one of the most effective meta-heuristics for global optimization in continuous multidimensional spaces. It is in the class of the Genetic Algorithms and organizes the search for sub-optimal solutions in a population. Inspired by the ideas in natural evolution, it has three common operators - selection, crossover, and mutation. During selection, better-fitted individuals from the population are selected to reproduce hoping that the offspring will be even better. The crossover is applied to achieve an exploration of the multidimensional space of the solutions. On the other side of recombination is the mutation which is used for exploitation of the multidimensional solutions space. This researcher proposes a partial curve fitting for mutation improvement.

Partial Curve Fitting in Multidimensional Space

Curve fitting is a well-known approach in the fields of interpolation, approximation, and forecasting. The most popular form of curve fitting is linear regression where a single line is drawn at a minimum distance from a set of points. Generalized linear regression is an approach to map nonlinear curves in the calculations done for linear regression. With modern computers generalized linear regression is successfully replaced with nonlinear regression models. The most popular nonlinear models are logarithmic, exponential, and polynomial.

In a multidimensional space, where $y = f(\vec{x})$ and $\vec{x}$ is a vector, set of function $y = f_i(x_i)$ can be defined. Functions f_i are not interesting by themselves. The way in which curve fitting can be applied over these functions is the interesting part. By applying nonlinear regression best fitting curve from the set of logarithmic, exponential, and polynomial is selected to approximate each function f_i.

Proposition for Differential Evolution Mutation

The classic form of mutation uses a difference vector calculated from randomly selected individuals. In the proposed modification an approximate function (obtained by nonlinear regression) is used for each f_i. The difference vector is checked element by element and each value that not corresponds with the gradient of the approximating function is inverted. By such an extension of the mutation partial derivative helps for the better approaching the global optimum(s).

Conclusions

This research proposes curve fitting motivated modification of the mutation operator in Differential Evolution. The proposed mutation shows promising improvements in the optimization convergence compared with the classical way of mutation.

Acknowledgments This work was inspired and supported by private funding of Velbazhd Software LLC.

Bounds for BER of Integer Coded Hexagonal QAM in AWGN Channel

Hristo Kostadinov, Nikolai Manev

We investigate the performance of coded modulation scheme based on the application of integer codes to hexagonal quadrature amplitude modulation (QAM). An upper and a low bound for bit error probability (BER) in the case of AWGN channel are derived. These bounds are very close so it makes the calculation of the exact value of BER unnecessary in practice.
We investigate the performance of coded modulation scheme based on the application of integer codes to hexagonal quadrature amplitude modulation (QAM). An upper and a low bound for bit error probability (BER) in the case of AWGN channel are derived. These bounds are very close so it makes the calculation of the exact value of BER unnecessary in practice.

1 Introduction

The term coded modulation means a combination of a scheme of coding and modulation techniques. Nowadays, in modern digital communication systems, high-order modulation is preferred for high-speed data transmission. One of the most popular modulation in commercial communication systems is square quadrature amplitude modulation (SQAM). SQAM scheme is easy to be implemented and has a good performance with simple detection.
Recently, the hexagonal quadrature amplitude modulation (HQAM) was proposed. A comparison of the two constellation, SQAM and HQAM, shows that HQAM is more power efficient than SQAM and preserves low detection complexity. In [1, 2] was derived the general formula calculating the average energy per symbol of the HQAM. Also, in the same work was analysed the bit error rate (BER) of the HQAM over AWGN channel, without using any coding techniques.
Integer codes are codes defined over finite rings of integers. Their advantage over the traditional block codes, is that we can correct errors of a given type, which means that for a given channel and modulator we can choose the type of the errors (which are the most common) and after that construct integer code capable of correcting those errors. The application of integer codes in different modulation schemes, especially in QAM, are discussed in [3, 4, 5, 6]. In this work bounds for the BER of SQAM and HQAM over AWGN channel will be shown. Examples of 16, 64, 256-HQAM coded by integer code shall be presented.
Before finding tight bounds of BER for HQAM, we have investigated BER of SQAM. The reason is, that for SQAM we have the exact expression of BER.

References

[1] Sung-Joon Park: Triangular quadrature amplitude modulation, IEEE Commun. Lett., vol. 11, no. 4, 292–294 (2007).

[2] Sung-Joon Park: Performance Analysis of Triangular Quadrature Amplitude Modulation in AWGN Channel. IEEE Commun. Letters, Vol. 16, 765–768 (2012).

[3] H. Kostadinov, H. Morita and N. Manev: Integer Codes Correcting Single Errors of Specific Types ($\pm e_1, \pm e_2, \ldots, \pm e_s$), IEICE Trans. on Fundamentals, Vol. E86-A (7), 1843–1849 (2003).

[4] H. Kostadinov, H. Morita and N. Manev: Derivation on Bit Error Probability of Coded QAM using Integer Codes. IEICE Trans. on Fundamentals, Vol. E87-A (12), 3397–3403 (2004).

[5] H. Kostadinov, H. Morita, N. Iijima, A.J. Han Vinck and N. Manev: Soft Decoding of Integer Codes and Their Application to Coded Modulation, IEICE Trans. on Fundamentals, Vol. E39-A (7), 1363–1370 (2010)

[6] H. Kostadinov, H. Morita, N. L. Manev: On (-1,+1) Error Correctable Integer Codes, IEICE Trans. Fundamentals, vol. E93-A (12), 2758–2761 (2010).

Computational study of the aggregation behaviour of antimicrobial peptides

E. Lilkova, N. Ilieva, P. Petkov, L. Litov

Antimicrobial peptides (AMPs) are naturally occurring molecules, that are released by almost all forms of life as part of the innate immune response of the host. They are small, structurally diverse proteins of a mainly cationic and amphiphilic nature. AMPs display antimicrobial activity against a broad spectrum of both Gram-positive and Gram-negative bacteria, fungi, parasites, and even some viruses. Notably, so far bacteria have not succeeded to develop efficient resistance against their action, which makes AMPs a promising therapeutic alternative to the conventional small molecule antibiotics.

The proper understanding of the antimicrobial action of AMPs is still an open problem in modern science. It is generally accepted, that their bactericidal activity results from their interaction with the target bacterial membrane. There are several models, that try to explain this interaction, however, multiple aspects of it are still controversial, including which is the biologically active secondary structure of the particular AMP, how do the they adopt it and what is the AMPs behavior in bodily liquids prior to attacking the target membrane.

Here, we employ different computational molecular modelling approaches and simulations to investigate the solution behavior several different AMPs of a particular class — linear AMPs. The studied peptides have different secondary structures – α-helical (magainin 2 [1], bombinin H2 [2]), unstructured (indolicidin [3]) as well as a number of newly isolated peptides from the mucus of the garden snail *Cornu Aspersum*) of yet unresolved experimentally structure [4]. By means of molecular dynamics (MD) simulations we demonstrate that linear AMPs tend to self-associate in clusters in solution, prior to their interaction with the target membrane, and this process also drives their convergence into the biological fold.

Our results demonstrate that the secondary structure of monomeric linear α-helical AMPs in solution is not stable [1, 2] and they usually adopt a conformation, that is not the most favorable for exerting their biological activity. Nonetheless, it should be noted that naturally AMPs are not released as monomers in solution, but are part of multicomponent secretory fluids (mucus), exhibiting certain biological activity. When in solution with multiple AMP monomers, the peptides quickly start to self assemble in clusters [2, 3]. This aggregation process drives a significant portion of the peptide chains to permanently transition their biologically active conformation prior to attacking the bacterial membrane, by providing the necessary amphypathic environment mimicking the membrane–solvent interface [2](Fig. 5a).

Our hypothesis, that self-assembly and aggregation-driven folding are the mechanism by which AMPs reach the target membrane in a functional folded state, was also tested on ten newly discovered AMPs [4]. Mono- and multicomponent solutions were prepared and studied using MD simulations. Again, the AMPs quickly self assemble into clusters, which size and properties depend on the composition of the solution, but the aggregates consist of a non-polar hydrophobic core, covered with charged or polar residues (Fig. 5b). Aggregation allows for increase in the number of inter-peptide hydrogen bond, which promotes formation of new and stabilizes already formed secondary structure elements.

Acknowledgements This work is partially supported by by the Bulgarian Science Fund (Grant KP-06-OPR 03-10/2018) and by the Bulgarian Ministry of Education and Science (Grant D01-323/18.12.2019) under the National Research Programme "Innovative Low-Toxic Bioactive Systems for Precision Medicine (BioActiveMed)" approved by DCM #

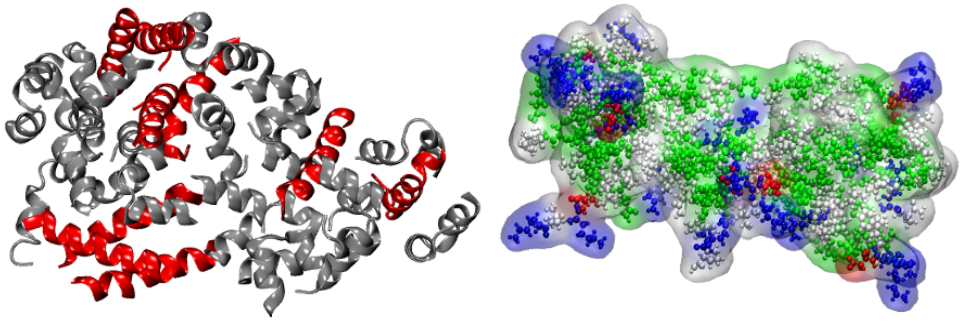

(a) (b)

Figure 5: (a) Bombinin H2 aggregate. Peptides in linear all-α-helical state are colored in red. (b) Multicomponent aggregate of peptides p5 and p7 [4]. Hydrophobic residues are colored in white, polar in green, basic in blue and acidic in red.

658/14.09.2018. Computational resources were provided by the BioSim HPC Cluster at the Faculty of Physics at Sofia University "St. Kl. Ohridski", Sofia (Bulgaria) and by CI TASK (Centre of Informatics – Tricity Academic Supercomputer & networK), Gdansk (Poland).

References

[1] Petkov, P, Marinova, R, Kochev, V, Ilieva, N, Lilkova, E, Litov, L. Computational study of solution behavior of magainin 2 monomers. Journal of Biomolecular Structure and Dynamics, (2019), 37(5), 1231-1240.

[2] Petkov, P., Lilkova, E., Ilieva, N., Litov, L. Self-Association of Antimicrobial Peptides: A Molecular Dynamics Simulation Study on Bombinin. International Journal of Molecular Sciences, (2019), 20(21), 5450.

[3] Marinova, R, Petkov, P, Ilieva, N, Lilkova, E, Litov, L. Molecular Dynamics Study of the Solution Behaviour of Antimicrobial Peptide Indolicidin. In: Georgiev K., Todorov M., Georgiev I. (eds) Advanced Computing in Industrial Mathematics. BGSIAM 2017. Studies in Computational Intelligence (2019), 793, 257-265.

[4] Ilieva, N., Petkov, P., Lilkova, E., Lazarova, T., Dolashki, A., Velkova, L., Dolashka, P., Litov, L.. In Silico Study on the Structure of Novel Natural Bioactive Peptides. Large-Scale Scientic Computing. LSSC 2019. Lecture Notes in Computer Science (2020), 11958, 332-339.

Markov type inequalities and extreme zeros of orthogonal polynomials

Geno Nikolov

By $\mathcal{P}_n$ and $\mathcal{P}_n^{\mathbb{C}}$ we denote the set of real and complex algebraic polynomials of degree not exceeding n. The inequalities of the form

$$\|p'\| \le c_n \|p\|, \quad p \in \mathcal{P}_n \quad \text{or} \quad p \in \mathcal{P}_n^{\mathbb{C}}, \tag{24}$$

which hold for various norms, are called Markov–, or Markov–Bernstein–type inequalities. Andrey Andreevich Markov (1889) settled the classical case of real polynomials and the uniform norm in $[-1,1]$. Precisely, he showed that in this case the Chebyshev polynomial of the first kind, $T_n(x) = \cos n \arccos x$, $x \in [-1,1]$, is the only (up to a constant factor) extremal polynomial and the best, that is, the smallest possible constant c_n is equal to $T_n'(1) = n^2$. Vladimir Andreevich Markov (1892) extended inequality (24) to higher order derivatives, showing that the extremality of the Chebyshev polynomials persists in this case, too. For the intriguing story of the inequality of the Markov brothers and some of its proofs we refer to the survey

A. Yu. Shadrin, Twelve proofs of the Markov inequality, In: *Approximation Theory: a volume dedicated to Borislav Bojanov*, Prof. Marin Drinov Academic Publishing House, Sofia, 2004, pp. 233–298.

For more than 130 years inequalities of Markov type proved to play an important role in Approximation Theory, they have been a challenge for many outstanding mathematicians and subject to various generalizations.

A natural goal is to try finding the sharp Markov constant

$$c_n = \sup\{\|p'\|/\|p\| \ : \ p \in \mathcal{P}_n, \ p \not\equiv 0\}\,.$$

However, this turns out to be a rather difficult task, and so far only in a few cases it has been determined explicitly. Further reasonable objectives are to:

1. Find tight two-sided bounds for the sharp Markov constant
$$\underline{c}_n < c_n < \overline{c}_n\,.$$
2. Determine the correct order γ of the sharp Markov constant,
$$c_n = \mathcal{O}(n^{\gamma})\,, \quad n \to \infty\,.$$
3. Find the asymptotic Markov constant $c = \lim\limits_{n\to\infty} \dfrac{c_n}{n^{\gamma}}$.

When one considers the norm in a Hilbert space, the sharp Markov constant c_n admits a simple characterization: it is the largest singular value of a certain matrix. Despite this fact, even in L^2–norms induced by the weight functions of Jacobi ($w_{\alpha,\beta}(x) = (1-x)^{\alpha}(1+x)^{\beta}$, $x \in [-1,1]$, $\alpha, \beta > -1$), Laguerre ($w_{\alpha}(x) = x^{\alpha}\, e^{-x}$, $x \in (0,\infty)$) and Hermite $w_H(x) = e^{-x^2}$, $x \in (-\infty,\infty)$), the sharp Markov constants is known only in in the Hermite case (which is a trivial one) and in the classical Laguerre case $w(x) = e^{-x}$ (P. Turán (1960)).

The talk is centered around the Markov inequalities in the L^2 norms induced by the Laguerre and Gegenbauer weight functions, and includes:

- A brief account on the known results on the Markov inequalities with the Laguerre and Gegenbauer weight functions;
- Techniques for derivation of two-sided estimates for the sharp Markov constants in L^2-norms;
- Recent results on the the Markov inequalities with the Laguerre and Gegenbauer weight functions. Our two-sided estimates identify the sharp Markov constant, roughly, within a factor of $\sqrt{6} < 2.5$ in the Laguerre case, and a factor of 2 in the Gegenbauer case;
- A class of extremal problems in a Hilbert space. A relation between the sharp Markov constant with the Laguerre and Gegenbauer weight function and the extreme zeros of orthogonal polynomials;
- The Euler-Rayleygh method as a tool for derivation of two-sided estimates for the extreme zeros of orthogonal polynomials, and thereby of the sharp Markov constants;
- A discrete weighted Markov-Bernstein inequality and the extreme zeros of orthgonal polynomials.

The results are obtained in collaboration with Alexei Shadrin (Cambridge University, UK), Dimitar K. Dimitrov (State University of Sao Paolo, Brazil), my colleague Rumen Uluchev (Sofia University) and my former PhD student Dragomir Aleksov.

Closing Topograhic Survey Polygons with Inexact Angle Measurements

Tzvetan Ostromsky

A topograhic polygon is a geometric figure, consisting of points (stations) and connecting vectors, used to determine with maximum precision the shape of certain geographical object on the map. The polygon is "closed" if its initial and last points are the same or their exact position on the map is known in advance, otherwise it is "open". In general, the word "traverse" means "passing across". In surveying, this word is mainly used to denote the process of determining the lengths and directions of consecutive edges in the surveyed topograhic polygon. In dependence with the surveying instruments and method used, there are various kinds of traversing (chain traversing (by chain angle), compass traversing , theodolite traversing, etc.)

Here we consider closed compass polygons, in which the vector directions are measured by a compass. Such polygons are often used to survey some underground or hidden objects, not easy to access (tunnels, mine galleries, caves, canyons, etc.). If the object is flat, then only the distance and the azimuth is measured for each vector (2D case). Otherwise, in general (3D case), the slope of each vector should be measured too.

If all the measurements in a closed traverse are exact, then the sum of all vectors of the survey must be zero. In practice, however, this does not happen. Due to various reasons, as for instance, the limited precision of the measurement instruments, this sum (called here "displacement error /vector") is not zero in general (causing a problem to place precisely all stations on the map). In order to resolve this problem, several adjustment methods have been developed, having respectively their advantages and disadvantages. Each method adjusts in some proper way (following certain assumptions) the traverse measurements taken in order to get rid of the displacement error. The final goal is to close exactly the polygon (which is required in some critical practical applications).

One "classical" solution of the polygon closing problem, which is rather straightforward and easy to implement, is the so-called *Graphic method*. The Graphic method causes each vector of the polygon to be adjusted by a part of the displacement error, proportional to its length. This procedure changes both the lengths and the angles of the polygon vectors. Another, more complicated method is the *Bowditch's method*. It is based on the assumption that the errors in linear measurements are proportional to their lenght and that the errors in angular measurements are inversely proportional to the square root of the length of the line. Bowditch's method is mostly used to balance a traverse where linear and angular measurements are of equal precision. *Transit method* is yet another approach to the problem, which may be advantageous where angular measurements are more precise that the linear measurements. In many practical situations, however, this is not the case. The new affordable laser meters made it easy to increase rapidly the precision of distance measurements, while this is not the case for the azimuth measurements (additionally, some system errors occur sometimes in the latter). Therefore our approach to the above problem is more conservative to the distance measurements than to the angles (esp. azimuth measurements). In other words, our task in the solution of the above general problem will be to find a way to close traversing surveys by adjustment of angular measurements only (without changing the distances). A solution of that task is proposed in this talk.

Framing the structural space in entropy and hierarchy

Iliyan Petrov

Introduction. The complexity of systems and the evolution in their structures are among the most challenging areas in scientific research. The quantitative assessment and qualitative classification of structures require objective and balanced methods for analyzing the large volumes of information related with the dynamics of resource distributions and events probabilities.

1. Indicators for system complexity. The complexity of systems is measured in the concepts of entropy and hierarchy by specific composite indicators. At the first level, the input data about the relative weights p_w of system's components are "transformed" by some basic functions: $\varepsilon(p_w)$ - for entropy, and, $\iota(p_w)$ - for hierarchy. The second level is universal as approach for any basic function - it summarizes the output results from first level for obtaining an aggregated assessment about the whole system.

Information theory and Shannon Entropy (SE) assess system complexity in the context of variety and diversity with the Shannon-Wiener Index (SWI): $\varepsilon_S(p_w) = -p_w \log_b(p_w)$ [1]. High values of $\Sigma_{w=1}^{N} \varepsilon_S(p_w)$ reflect configurations with large number of elements and distributions with small relative weights. SWI produces similar hyperbolic concave profiles for all logarithm basis values "$b > 1$" . Logically, lower values of "b" inflate more the volume of information at micro and macro level. All profiles have a maximum at $p_w = 0.37$ - a fact that creates ambiguity in interpretation for relative weights bellow and above that maximum.

Hierarchy (concentration) assesses complexity in terms of order and domination based on accumulation of resources among smaller number of components - therefore the basic functions monotonically and non-linearly increase in the interval $p_w \in [0, 1]$.

In Herfindal-Hirschman Index (HHI) the quadratic function $\iota(p_w) = p_w^2$ produces exponential profile, which underestimates small and overestimates large components [2].

To improve the quality of research we developed an original concept for assessing order and domination in system structures with a model called "Petrov Hierarchy Indicator (PHI)" [3]: $\iota_P(p_w) = \frac{p_w}{1+\left[(\Sigma_{j=1}^{J} log_{R_j}(p_w)/J)\right]^c}$; where: p_w - relative weight of the w^{th}system component; R_j - referral weights ; J - number of referral weights; c - interaction intensity. PHI allows to define whole families of monotonically increasing functions with S-curves while experiments lead to select a "golden section" with following values:

$J = 2; R_1 = 0.001$, $R_2 = 0.25$; $c = 2$; $\Rightarrow \iota_{P(log:0.001;0.25)} = \frac{p_w}{1+[(log_{0.001} p_w + log_{0.25} p_w/2]^2}$.

2. Framing structural space in entropy and hierarchy. For enhancing the analysis of complexity and evolution systems structures we introduce objective original approaches for framing information space based on the symmetry and asymmetry for distribution of resources with two new parameters - "Transition Step $\Delta p(TS)$", and "Distribution Step - $\Delta p(DS)$". For hierarchy full symmetry/equality of relative weights of elements means minimum hierarchy/concentration, while for entropy - maximum diversity.

a) Symmetry (equality) of components defines the concept for the production of absolute maximum levels of entropy and corresponding absolute minimum levels hierarchy in a scenario described as *"Active competition with equalization within all populations"*.

b) Asymmetry (inequality) of components produces of working levels with minimum entropy and corresponding maximum hierarchy described as a scenario called *"Week competition with single domination in all populations"*.

Complexity indicators $\int_0^1$	Basic	Symmetry	Asymmetry	Space
Transition step $\Delta p(TS)$	0.01	0.01	0.01	0.01
Distribution step $\Delta p(DS)$	-	0.01	0.001	-
Petrov Hierarchy $\iota_{P(log;0.001;0.25)}$	0.467	0.798 (min)	0.963(max)	0.165
Herfindahl Hierarchy ι_H	0.333	0.448(min)	0.905(max)	0.457
Shanon Entropy $\varepsilon_{S(log2)}$	0.361	0.16(max-norm)	0.07(min-norm)	0.09

c) Working space of structural information. The combination of symmetric and asymmetric transition paths enclose an area whose quadrature can be easily calculated as a difference between the information integrals of Maximal and Minimal Entropy or Hierarchy. This area can be considered as the "Working Structural Space" where may happen the evolution system complexity in real conditions. Within that space, we can trace different projection paths for mean (arithmetic, geometric, etc.) entropy or hierarchy in system configurations.
3. Comparing information integrals of entropy and hierarchy on micro and macro levels.
a) Information quadrature at micro level for basic functions. Being continuous in the entire interval for $p_w \in [0, 1]$, all discussed transform functions can be differentiated and defining their quadrature by symbolic integration is a possible with a maximum level of accuracy.
b) Information quadrature at macro level for maximums and minimums of entropy and hierarchy are calculated with high level approximation according Riemann's approach [4]. The table here-below displays the integrals values for the 4 most important aspects: basic functions; minimum hierarchy and maximum entropy based on symmetry; maximal hierarchy and minimum entropy based on asymmetry; and, the "structural working space".
Discussion and conclusions. The mathematical analysis of discussed indicators by comparing their integrals at micro and macro levels provides very strong evidences that *Petrov Hierarchy* is significantly superior than traditional indicators (*Herfindahl Concentration* and *Shannon Entropy*). The well balanced and flexible *Petrov Hierarchy* provides new possibilities for comprehensive analysis of systems' complexity in larger number of areas.

References

[1] Shannon, C. E., Weaver.W., 1948. A mathematical theory of communication. The Bell System Technical Journal, 27, 379–423 and 623–656

[2] Herfindahl, O. C., 1950. Concentration in the U.S. Steel Industry. Unpublished doctoral dissertation, Columbia University.

[3] Petrov, I.I., 2015. Structural Evolution of World and European energy markets and the development of gas pipeline networks in South-East Europe with participation, Ph.D. dissertation, Russian State University for oil and gas "I.M. Gubkin", Moscow, Russia.

[4] Riemann, B. (1854), "About the description of a function by arbitrary functions".

A comparative survey on Neural Rendering

Kalin Presnakov, Stanislav Harizanov

Generative adversarial networks (GANs) show remarkable results in image synthesis, though they don't allow for explicit output control. *Neural rendering* is a new interdisciplinary field which combines methods from deep learning, computer graphics and computer vision — classical rendering approaches of computer graphics are used alongside with approaches based on deep generative models with the purpose of *controlled* synthesis of novel images. Unlike classical GANs which take as an input samples from a noise prior the methods of neural rendering enable usage of input images or other conditional scene-dependent input. The output is a photo-realistic image that is conditioned on the input. The field is an emerging one and as a consequence the applications are diverse and the methods somewhat scattered. Deep models that are used are usually conditional GANs (cGANs), but also variational autoencoders (VAE) or other encoder-decoder based models. Neural rendering techniques differ on their level of explicit/implicit control, input, output, usage of classical graphical modules, multimodality of the output, generality. Our aim is to present a comparative literature survey with an emphasis on some classes of problems that are being solved by neural rendering. We'll showcase some excellent results we've came across on applications like semantic image synthesis, semantic image manipulation, improving the realism of synthetic renders, approximating expensive rendering techniques like ambient occlusion, subsurface scattering and global illumination, novel view synthesis from multi-planar images, relighting, reenactment techniques and others. We also aim to present a background on some widespread network architectures and other tools used in the field, input variants, loss functions and learning strategies.

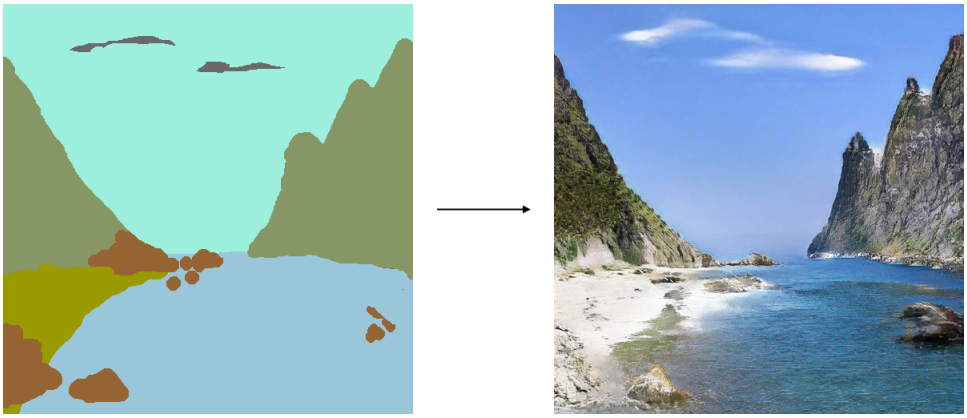

Figure 6: Semantic image synthesis by a semantic map (left). Each color in the semantic map is denoting a type of a region in the output image (right) like sea, sky, mountain, etc. The image was obtained by using an online tool showcasing the GauGAN architecture by NVidia Research.

Acknowledgment: The partial support through the Bulgarian NSF Grant number DN11/9-15.12.2017 is highly acknowledged.

Shilnikov chaos in a Dynamical Sytem of Three Competing Economic Sectors

Denislav Serbezov, Elena Nikolova

In this study we extend a basic dynamical model, proposed in [1], which describes competition between the public sector and the private sector. We add a new ordinary differential equation to the basic system, which describes dynamics of non-governmental organizations (NGOs) sector, assuming that the NGOs sector competes also with the aforementioned two sectors. For our convenience we reduce the number of system parameters and analize dynamical properties of the equilibrium points of the three–dimensional system for selected values of its parameters. On the basis of this analysis we identify two equilibrium points of the system which evolution corresponds to development of chaos of Shilnikov kind [2]. We find that a such chaos in the three–sector interaction system occurs for the case, in which the private sector dominates on the progress of the public sector and NGOs sector vanishes. We illustrate numerically the development of a chaotic system attractor with increasing the value of an appropriate control parameter.

References

[1] D. Dendrinos. The dynamics of cities: Ecological determinism, dualism and chaos, Routledge, London, 1992.

[2] L. P. Shilnikov. A case of the existence of a denumerable set of periodic motions, Sov. Math. Dokl., **6** (1965), 163–166.

Comparison of four classification methods on high-dimensional small-sample-size synthetic NGS data

Felitsiya Shakola, Valeriya Simeonova, Ivan Ivanov

A large number of applications spanning various fields, such as gene expression analysis, computer vision, finance, and weather prediction, has been developed to extract insight from high-dimension small-sample-size data sets. The latter present great challenge for conventional statistical analysis and current machine learning methods [1].

One of the main goals of translational bioinformatics is the use of high-throughput measurements for the development of classifiers that can identify different phenotypes that are manifested as a result of the interaction of the organism's genotype and environmental factors [2]. From this perspective, classification analysis is a type of supervised learning that extracts models describing classes that are relevant to a phenotype of interest. These models, called classifiers, predict the belonging of a data point to categorical (discrete) classes. An example is a classifier categorizing cells as tumour or normal. RNA-Seq data is produced by next generation sequencing (NGS). Specifically, small fragments of messenger RNA produced as a result of gene expression are sequenced. Those RNA fragments are cleaved at random, converted to DNA sequences, and the results are summarized as reads [3]. After obtaining the reads they are mapped against a reference genome to determine the levels of gene expression. The number of reads mapped to a gene in the reference genome is a discrete measure of gene expression levels.

The genomic data sets are high-dimensional — with 20,000 or more features, while the number of tested samples/patients is often restricted to a few hundred or less, due to high per sample cost or rarity of phenotype. This means that the training and testing processes of the classification have to be performed on the same data set, where standard deviation, variance, and lack of correlation with the true error can seriously impair error estimation. Synthetic data generation models are used in this case to model the behaviour of real gene expression. It is accepted in the scientific community that the multivariate Gaussian distribution is optimal for modelling the expression of messenger RNA [4, 5, 6]. Starting with this hypothesis, synthetic RNA-Seq data are generated, by applying a specific nonlinear Poisson transformation to the expression of messenger RNA model [7]. These synthetic data sets provide the opportunity to study the classification accuracy and to compare the performance of various classification rules.

Our work examines the influence of different model parameters for the generation of synthetic RNA-Seq data on several classification rules. The variation of parameters for the data generation includes: the amount of global markers, representing genes related to a state or a disease, i.e. biomarker genes; dispersions of the gene expression levels; and the correlation between expression levels and class membership. We comparted the performance of four classification rules, linear discriminant analysis (LDA), k-nearest neighbours (KNN), support vector machine (SVM), and artificial neural networks (ANN) on synthetic data sets of 50, 150 and 300 samples based on 300 features/genes. We used portions of the generated data for training of the classifiers and the remaining samples for testing of the error rates.

The estimation of the classification accuracy is assessed using two strategies. The first involves the classification confusion matrix and quantities related to it: true positive rate (TPR), true negative rate (TNR), positive predictive value (PPV), error rate (ER), and the

respective receiver operating characteristic (ROC) curves for the classifiers. The second accuracy assessment approach uses the bolstered error estimation (bresub) [8]. This approach is particularly useful in the case of small number of available samples. The bresub error estimation results are compared to the classification accuracy information provided by the confusion matrices.
Importantly, with the increase of the number of training samples, the number true biomarker genes, and strength of their mutualistic relationships as measured by the corresponding covariance matrix, the accuracy of the classification increases. Our comparative results show that SVM is the most accurate classifier in the majority of the considered simulated data scenarios. However, LDA's accuracy is the highest in most of the cases with a relatively small number of training samples. These results suggest that LDA could be recommended as an accurate and at the same simple classification rule for real biological data with a small number of available samples; thus, avoiding potential overfitting issues in such cases.

References

[1] Iain M. Johnstone and D. Michael Titterington. Statistical challenges of high-dimensional data. *Philosophical Transactions of the Royal Society A: Mathematical, Physical and Engineering Sciences*, 367(1906):4237–4253, November 2009.

[2] R B Altman. Translational bioinformatics: Linking the molecular world to the clinical world. *Clinical Pharmacology & Therapeutics*, 91(6):994–1000, May 2012.

[3] Ali Mortazavi, Brian A Williams, Kenneth McCue, Lorian Schaeffer, and Barbara Wold. Mapping and quantifying mammalian transcriptomes by RNA-seq. *Nature Methods*, 5(7):621–628, May 2008.

[4] Jianping Hua, Waibhav D. Tembe, and Edward R. Dougherty. Performance of feature-selection methods in the classification of high-dimension data. *Pattern Recognition*, 42(3):409–424, March 2009.

[5] S. Attoor, E. R. Dougherty, Y. Chen, M. L. Bittner, and J. M. Trent. Which is better for cDNA-microarray-based classification: ratios or direct intensities. *Bioinformatics*, 20(16):2513–2520, September 2004.

[6] Lori A. Dalton and Edward R. Dougherty. Application of the bayesian MMSE estimator for classification error to gene expression microarray data. *Bioinformatics*, 27(13):1822–1831, May 2011.

[7] Noushin Ghaffari, Mohammadmahdi R Yousefi, Charles D Johnson, Ivan Ivanov, and Edward R Dougherty. Modeling the next generation sequencing sample processing pipeline for the purposes of classification. *BMC Bioinformatics*, 14(1), October 2013.

[8] Ulisses Braga-Neto and Edward Dougherty. Bolstered error estimation. *Pattern Recognition*, 37(6):1267–1281, June 2004.

On to Parallel MLMC for Stationary Single Phase Flow Problem

Nikolay Shegunov, Oleg Iliev

Many problems that incorporate uncertainty often require solving a Stochastic Partial Differential Equation. Fast and efficient methods for solving such equations are of particular interest for Computational Fluid Dynamics(CFD) and more precisely for problems involving porous media flows. It is believed that with the advances of the hardware and the development of efficient algorithms a breakthrough is possible for this class of problems. For example one could imagine a simulation of a subsurface water flow in an area of hundreds of square km, characterized by highly varying uncertainty permeability. The approach which can serve as a basis for developing efficient algorithms for such problems is the Multilevel Monte Carlo method. It is a generalization of a well known class of computational methods that relies on repeated random sampling, namely, Monte Carlo Method. The idea of the particular MLMC which we consider is to sample not only from the fine grid SPDE, where the solution is demanded, but also from approximations of the SPDE on coarser grids. MLMC overcomes the slow convergence rate of the classical MC method, thanks to the multilevel sampling. However, the parallelization of MLMC becomes much more involved then the parallelization of the classical MC approach, because the problem for finding optimal processor distribution in the most general form is NP complete [1]. In this paper we consider a stationary single phase flow through random porous medium as model problem and explore different scheduling strategies. Although a simple model, this problem is well established test case in the field because shows well the computational challenges of such models. The construction of MLMC algorithm requires tree main steps: generation of correlated random number generator for the permeability field, numerical scheme for discretization of the PDE for each realization of the permeability, and coarse grain method that approximates the solution at the coarser levels. We follow the work of [2], and use Circulant Embedding approach as a random field generator, cell centered finite volume method for numerical discretization and simplified renormalization as coarse graining approach.

The authors gratefully acknowledge the Gauss Centre for Supercomputing e.V. (www.gauss-centre.eu) for funding this project by providing computing time on the GCS Supercomputer SuperMUC at Leibniz Supercomputing Centre (www.lrz.de).

References

[1] D. Drzisga, B. , Gmeiner , U. Rude, R. Scheichl, SIAM J. SCI. Comput., Scheduling Massively Parallel Multigrid For Multilevel Monte Carlo Methods

[2] Oleg Iliev, Jan Mohring, Nikolay Shegunov, LSSC, Renormalization Based MLMC Method for Scalar Elliptic SPDE

Application of Hierarchical Semi-Separable compression for solving 2D elastodynamic problem of a finite-sized solid containing cavities

Slavchev, D., Margenov, S., Georgiev, I.

Wave propagation in solids containing heterogeneities like elastic or rigid inclusions or cavities is one of the fundamental problems in mechanics. The heterogeneities act as both wave scatterers and stress concentrators. This makes the problem of the dynamic behavior of an elastic solid, that contains multiple cavities an important problem in many technological fields like material science, non-destructive testing evaluation, computational geophysics and fracture mechanics. The Boundary Integral Equation Method (BIEM) is used for solving this problem, following [1]. We are using a Matlab® program provided by the authors of that paper – Parvanova, Dineva and Manolis, to generate the system of linear equations.
The BIEM of the problem is formulated as:

$$c_{ij}u_j(\mathbf{x},\omega) = \int_\Gamma U^*_{ij}(\mathbf{x},\mathbf{y},\omega)t_j(\mathbf{y},\omega)d\Gamma - \int_\Gamma T^*_{ij}(\mathbf{x},\mathbf{y},\omega)u_j(\mathbf{y},\omega)d\Gamma,$$

where c_{ij} is the jump term determined by the geometry at the collocation point, $\mathbf{x} = (x_1, x_2)$ and $\mathbf{y} = (y_1, y_2)$ are position vectors of the source and the field points, $u_j(x)$ is the displacement and $t_j(x)$ is the traction at the boundary, U^*_{ij} and T^*_{ij} are the displacement fundamental solution and the traction fundamental solution of the governing equation.
The entire boundary is discretized by quadratic boundary elements, followed by nodal collocation. After the boundary conditions are satisfied, the BIEM equations are transformed into a system of linear algebraic equationss:

$$\mathbf{G}\cdot\mathbf{t} - \mathbf{H}\cdot\mathbf{u} = 0, \tag{25}$$

where $\mathbf{G}$ and $\mathbf{H}$ are the final global influence matrices. Both are dense $2m \times 2m$ matrices, where m is the number of boundary nodes. The global vectors $\mathbf{u}$ and $\mathbf{t}$ (both of size $2m$) contain the boundary displacement and traction components, respectively. Eq. 25 can then be rearranged into the standard linear algebraic equation form $Ax = B$.
The final system of linear equations is not completely dense, however an 128×128 example has a sparsity of only 3.6%. See Fig. 7. Solving dense systems of linear equations is a computationally expensive task. For example, the computational complexity of the traditional Gaussian elimination is an $O(n^3)$ in this case, n is the number of unknowns. An alternative is using Hierarchical compression to compress the matrix into a hierarchical matrix, that can be expressed in much smaller space and allows more efficient matrix operations to be carried over the compressed matrix. Here we consider the Hierarchically Semi-Separable compression (HSS) based algorithm implemented in the STRUctured Matrices PACKage (STRUMPACK)[2].
The HSS compression based solver uses three steps to solve the system of linear algebraic equations:

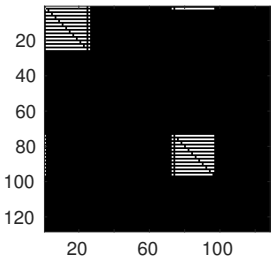

Figure 7: Sparsity of the problem matrix.

1. *Hierarchical Semi-Separable compression.* In this step the initial matrix A is compressed (approximately) in the compressed form H with:

$$A = \begin{bmatrix} A_{11} & A_{12} \\ A_{21} & A_{22} \end{bmatrix} = \begin{bmatrix} D_1 & U_1^{\text{big}} B_{1,2} V_2^{\text{big}*} \\ U_2^{\text{big}} B_{2,1} V_1^{\text{big}*} & D_2 \end{bmatrix},$$

where the U_i, B_{ij} and V_j are called *generators*. If the matrix A has suitable low-rank off-diagonal blocks U_i will be "tall" and "skinny", B_{ij} will be small and square and V_j will be "short" and "wide". The diagonal blocks D_i can be further compressed in a similar way and so on recursively. The generator matrices on different levels can be further expressed as:

$$U_3^{\text{big}} = \begin{bmatrix} U_1^{\text{big}} & 0 \\ 0 & U_2^{\text{big}} \end{bmatrix} U_3 \quad \text{and} \quad V_3^{\text{big}} = \begin{bmatrix} V_1^{\text{big}} & 0 \\ 0 & V_2^{\text{big}} \end{bmatrix} V_3,$$

which means that the $^{\text{big}}$ generators need only be computed at the lowest level of recursion. The computational complexity of this step is $O(nr^2)$, where r is the maximum rank of the off-diagonal blocks.

2. *ULV-like compression.* The algorithm inside STRUMPACK uses the structure of the compressed matrix H, while the original ULV factorization uses orthogonal transformations, hence the name ULV-like. It first solves $O(n-r)$ unknowns in reverse order of the HSS compression. At the highest level of recursion this leaves a dense system of $O(r)$ unknowns that is solved with LU factorization. The computational complexity is $O(nr^2)$.
3. Solution. In this step the factorized matrix and the right hand side are used to obtain the final solution. The complexity of this step is $O(rn)$

The numerical tests are ran on the Supercomputer AVITOHOL at the Institute of Information and Communication Technologies at the Bulgarian Academy of Sciences. We use one node with two Intel Xeon E 2650 v2 CPUs with a total of 16 cores. We compare the performance and accuracy of STRUMPACK and compare it with the Gaussian solver from Intel®'s Math Kernel Library[3].

References

[1] S. L. Parvanova, P. S. Dineva, and G. D. Manolis. Dynamic behavior of a finite-sized elastic solid with multiple cavities and inclusions using biem. *Acta Mechanica*, 224(3):597–618, Mar 2013.

[2] François-Henry Rouet, Xiaoye S. Li, Pieter Ghysels, and Artem Napov. A Distributed-Memory Package for Dense Hierarchically Semi-Separable Matrix Computations Using Randomization. *ACM Trans. Math. Softw.*, 42(4), June 2016.

[3] Intel®. Math Kernel Library. https://software.intel.com/en-us/intel-mkl.

Universal In-memory Computing on the Edge of Chaos

Angela Slavova and Ronald Tetzlaff

One of the key features of neural networks is the ability to compute with memory in the case computation is disturbed and performed with localized memory storage.In this work we shall present a special class of memristor Cellular Nonlinear/Nanoscale Networks (MCNN) operating on the edge of chaos. In general, a spatially continuous or discrete medium made of identical cells interacting with all cells located within a neighborhood exhibits complexity if the homogeneous medium can give rise to a non-homogeneous state or spatio-temporal pattern under some homogeneous initial and boundary conditions.
Throughout extensive simulations we shall present non-uniform spatial-pattern generation and we shall study the global motion of excitable waves. Applications in EEG signal generation will be shown in order to predict the epileptic seizures.

References

[1] Slavova, A., Tetzlaff, R., Zafirova, Z. Edge of chaos in nanoscale memristor CNN. IEEE Proc. ISCAS 2019, (2019)

[2] Slavova, A.Dynamics of a new hysteresis memristor CNN. IEEE Proc. ECCTD 2020 (2020)

[3] Slavova, A., Tetzlaff, T. Mathematical Analysis of Memristor CNN. ItechOpen, DOI: 10.5772/intechopen.86446, (2019)

[4] Slavova, A., Tetzlaff, R. Edge of chaos in reaction diffusion CNN model. Open Mathematics, vol.15, issue 1, (2017), https://doi.org/10.1515/math-2017-0002

iSybislaw – the Bibliographic Database of World Slavic Linguistics Publications: Structure and Functionalities of Bulgarian Language Content

Velislava Stoykova IBL-BAS, Pawel Kowalski ISS-PAS

The paper presents the structure of the bibliographic database of world Slavic linguistics publications iSybislaw. It offers a comparison of that database with some other bibliographic database and outlines its specific architecture and functionalities as being specialized in presenting multilingual online accessible source for bibliographic data search on Slavic linguistics research works. The functionalities of the iSybislaw module which contains Bulgarian language source of related linguistic bibliographic works is described as a part of its multilingual content and iSybislaw's overal structure.

The main iSybislaw system presents an Information Retrieval searchable database which architecture includes:

(1) hierarchical linguistic knowledge base – a conceptual knowledge base which uses linguistic concepts (subject) classification in synonymy conceptual relations hierarchy

(ii) multilingual electronic dictionary of keywords (multilingual terms for related linguistic concepts) in all Slavic languages – a multilingual terminological database

(iii) multilingual bibliographic database of world Slavic linguistics publications encoded according to specific metadata scheme and standards

The Bulgarian module of iSybislaw is developed over time and contains all the three parts in its architecture including the linguistic terminological database in Bulgarian language and constantly updated rich bibliographic database which is representative for Bulgarian linguistics. It combines the properties of terminological database with machine translation functionalities and allows to process query search in Cyrillic alphabet over all iSybislaw multilingual database according to various criteria. The Bulgarian module of iSybislaw, mainly its electronic keyword search options, allows to be used both as a tool for searching the related reference works in Slavic linguistics in a diachronic perspective and as a research tool for comparative Slavic studies.

Vector Schrodinger equation: Nonlinearity, Multidimensionality, Integrability. What to Prefer?

Michail D. Todorov

For a system of nonlinear Schrödinger equations (SCNLSE) coupled both through linear and nonlinear terms, we investigate numerically the head-on and taking-over collision dynamics of polarized solitons. In the case of general elliptic polarization, analytical solutions for the shapes of steadily propagating solitons are not available, and we develop an auxiliary numerical algorithm for finding the initial shape. We use a superposition of polarized solitons as the initial condition for investigating the soliton dynamics (sech-like as well as general form). We consider the interactions with and without cross-modulation, with stationary shapes and with breathers. For general nontrivial cross-modulation, a jump in the polarization angles of the solitons takes place after the collision (polarization shock). For moderate and large values of the nonlinear coupling parameter, additional solitons are created during the collision of the initial ones.

We also find that, depending on the initial phases of the solitons, the polarizations of the system of solitons after the collision change, even for trivial cross-modulation. This sets the limits of practical validity of the celebrated Manakov solution. In the majority of cases the solitons survive the interaction, preserving approximately their phase speeds and the main effect is the change of individual polarization but the total net polarization of the system is conserved. However, in some intervals for the initial phase difference, the interaction is ostensibly inelastic: either one of the solitons virtually disappears, or additional solitons are born after the interaction.

In the case of pure linear coupling the Manakov system is enriched by a linear coupling term with complex-valued coefficient and the individual solitons are actually either blowing or dispersing breathers. The momentum of the individual quasi-particles (QPs) is conserved while the masses of the individual QPs oscillate, but the sum of the masses for the two QPs is constant. Respectively, the total energy oscillates during one period of the breathing, but the average over the period is conserved. The individual and total polarization angles for the two QPs oscillate with different periods before and after the interaction. This extends to the case of breathing our earlier results about the conservation of the total polarization for the interaction of non-breathing solitons.

The results of this work elucidate the role of the linear and nonlinear couplings, the initial phase, and the initial polarization on the interaction dynamics of soliton systems in SCNLSE. For moderate and large values of the nonlinear coupling parameter, additional solitons are created during the collision of the initial ones. Depending on the initial phases of the solitons, the polarizations of the system of solitons after the collision change, even for trivial cross-modulation. All this sets the limits of practical validity of the celebrated Manakov solution. The Manakov system loses its full integrability and the approach for its study is numerical. All the numerical experiments and computer simulations are implemented by using a fully conservative difference scheme in complex arithmetic.

Some information about the transition from Manakov model to perturbed Vector Schrodinger equation can be obtained by the so-called Complex Toda chain (CTC). We detail an asymptotic description of the interaction between N solitons in adiabatic approximation. These original equations are perturbed by gain/loss terms, periodic, polynomial, single and composite well (hump) external potentials. The gain and loss are taken to balance so that the

solutions do not blow up or decay away. The distance between the solitons, however, is taken to be large, so that they only interact in their tails, which is the basis for the asymptotic analysis. The inverse of this large separation is the perturbation parameter. The evolution of the soliton parameters is governed by a discrete system related to the complex Toda Chain. We derive the corresponding perturbed complex Toda Chain (PCTC) models for both SCNLSE and Manakov model. We show that the soliton interactions dynamics for the PCTC models compares favorably to full numerical results of the original perturbed SCNLSE and Manakov model. Unfortunately, the cross-modulation in SCNLSE sets the limits of practical validity of the Manakov solution and corresponding CTCs.

Sensitivity Analysis of a Large-Scale Air Pollution Model by Using Highly Efficient Stochastic Approaches

Venelin Todorov, Ivan Dimov, Tzvetan Ostromsky, Stoyan Poryazov

The Unified Danish Eulerian Model (UNI-DEM) [4] is in the focus of our investigation as one of the most advanced large-scale mathematical models that describes adequately all physical and chemical processes. One of the most attractive features of UNI-DEM is its advanced chemical scheme — the Condensed CBM IV [5], which consider a large number of chemical species and numerous reactions between them, of which the ozone is one of the most important pollutants for its central role in many practical applications of the results. The calculations are done in a large spatial domain, which covers completely the European region and the Mediterranean, for certain time period. Different parts of the large amount of output data, produced by the model, were used in various practical applications, where the reliability of this data should be properly estimated. Another reason to choose this model as a case study here is its sophisticated chemical scheme, where all relevant chemical processes in the atmosphere are accurately represented. The influence of emission levels over three important air pollutants (ammonia, ozone, and ammonium sulphate and ammonium nitrate) over big European cities with different geographical locations is considered. Studies of relationships between input parameters and model outputs is very useful for determining the reliability of the model.

Variance-based methods are most often used for providing sensitivity analysis. Several sensitivity analysis techniques have been developed and used throughout the years [2]. In general, these methods rely heavily on special assumptions connected to the behaviour of the model (such as linearity, monotonicity and additivity of the relationship between input and output parameters of the model). Among the quantitative methods, variance-based methods are the most often used. The main idea of these methods is to evaluate how the variance of an input or a group of inputs contributes to the variance of model output. Two of the most commonly used variance-based methods were applied in our study: *Sobol approach* and *Fourier Amplitude Sensitivity Test (FAST)*. These were implemented by using Monte Carlo algorithms.

Quasi-Monte Carlo algorithms are based on quasirandom or low discrepancy sequences which are "less random" than a pseudorandom number sequence, but more useful for numerical computation of integrals in higher dimensions, because low discrepancy sequences tend to sample space "more uniformly" than random numbers.

Let $\mathbf{x}_i = (x_i^{(1)}, x_i^{(2)}, \ldots, x_i^{(s)})$ for $i = 1, 2, \ldots$. The star discrepancy is given by:

$$D_N^* = D_N^*(\mathbf{x}_1, \ldots, \mathbf{x}_N) = \sup_{\Omega \subset E^s} \left| \frac{\#\{\mathbf{x}_n \in \Omega\}}{N} - V(\Omega) \right|, \tag{26}$$

where $E^s = [0,1)^s$. Let

$$n = \ldots a_3(n), a_2(n), a_1(n)$$

be the representation of n in base b. The radical inverse sequence is given by:

$$n = \sum_{i=0}^{\infty} a_{i+1}(n) b^i, \;\; \phi_b(n) = \sum_{i=0}^{\infty} a_{i+1}(n) b^{-(i+1)} \tag{27}$$

and it is fulfilled that

$$D_N^* = O\left(\frac{logN}{N}\right). \tag{28}$$

The original **Van der Corput** sequence [3] is obtained when $b = 2$.
Some modifications of the Van der Corput sequence are studied in our numerical experiments. The modifications of the Van der Corput sequence is often used to generate a "subrandom" sequence of points which have a better covering property than pseudorandom points.
A discussion of the systematic approach for sensitivity analysis studies in the area of air pollution modelling has been given. The Unified Danish Eulerian Model (UNI-DEM) is used in this particular study. We study the sensitivity of concentration variations of some of the most dangerous air pollutants with respect to the anthropogenic emissions levels and with respect to some chemical reactions rates.
A comprehensive experimental study of highly efficient stochastic approaches based on the Van der Corput sequence and its modification with different bases for multidimensional integration has been done. A comparison with the Latin Hypercube Sampling (LHS) is given for the first time. The algorithms have been successfully applied to compute global Sobol sensitivity measures corresponding to the six chemical reactions rates and four different groups of pollutants. The numerical tests will show that the stochastic algorithms under consideration are efficient for the multidimensional integrals under consideration and especially for computing small by value sensitivity indices. Clearly, the progress in the area of air pollution modeling, is closely connected with the progress in reliable algorithms for multidimensional integration.

Acknowledgement. This work is supported by the Bulgarian National Science Fund under Projects DN 12/5-2017 "Efficient Stochastic Methods and Algorithms for Large-Scale Problems" and KP-06-M32/2 - 17.12.2019 "Advanced Stochastic and Deterministic Approaches for Large-Scale Problems of Computational Mathematics".

References

[1] I. T. Dimov, R. Georgieva. Multidimensional Sensitivity Analysis of Large-scale Mathematical Models, Springer Proceedings in Mathematics & Statistics 45, Springer Science+Business Media, New York, 2013, 137–156.

[2] A. Saltelli, Tarantola, S., Campolongo, F., Ratto,M.: Sensitivity Analysis in Practice: A Guide to Assessing Scientific Models. Halsted Press, New York (2004)

[3] Van der Corput, J.G. (1935), "Verteilungsfunktionen (Erste Mitteilung)" (PDF), Proceedings of the Koninklijke Akademie van Wetenschappen te Amsterdam (in German), 38: 813–821, Zbl 0012.34705

[4] Z. Zlatev, Computer treatment of large air pollution models, KLUWER Academic Publishers, Dorsrecht-Boston-London, 1995.

[5] Z. Zlatev, I. T. Dimov, Computational and Numerical Challenges in Environmental Modelling, Elsevier, Amsterdam, 2006.

Multi-Layered Intuitionistic Fuzzy Intercriteria Analysis on some Key Indicators Determining the Mortality of Covid-19 in European Union

Velichka Traneva, Stoyan Tranev

The concept of intuitionistic fuzzy ICrA, based on the apparatus of the IMs (see [2]) and IFPs (see [1, 3]), was introduced in [6]. It calculating pairwise dependencies between each pair of criteria for evaluation of objects. The method receives as input datasets of the evaluations of multiple objects against multiple criteria and returns as output a table of detected dependencies in the form of intuitionistic fuzzy pairs between each pair of criteria [7]. In the original problem formulation that leads to the idea of ICrA, measuring against some of the criteria is slower or more expensive than measuring against others, and the decision maker's aim is to accelerate or lower the cost of the overall decision making process by eliminating the costly criteria on the basis of these existing correlations [6]. The complexity of the ICrA algorithm is $O(m^2n^2)$, which is polynomial in mn [8]. Later the ICrA has been extended in a theoretical aspect for its application to two-dimensional interval-valued intuitionistic fuzzy evaluations, three-dimensional and multidimensional intuitionistic fuzzy data [5, 9, 12, 13], with a software application being developed (see [10, 11]), freely available from the website [15]. In the present paper is extended a form of three-dimensional ICrA (3-D ICrA) [12] to a form of three- dimensional multilayer ICrA (3-D MLICrA) in an uncertain environment. Here, the 3-D MLICrA approach is applied on the dataset of total deaths attributed to COVID-19 per 1,000,000 people and some key indicators of European Union countries determining this mortality, provided by European Centre for Disease Prevention and Control [16], for the data for the period from February to November, 2020. The comparative analysis of the correlation dependencies between the proposed basic indicators of countries and the number of deaths caused by COVID-19 has been performed in the paper after application of ICrA, Pearson's, Spearman's and Kendall's rank correlation analyzes to show the advantages of the proposed approach. The defined 3-D MLICrA can be expanded to retrieve information to other types of multi-dimensional data cubes [4].

Acknowledgements This work is supported by the project of Asen Zlatarov University under Ref. No. NIX-440/2020 "Index matrices as a tool for knowledge extraction".

References

[1] Atanassov, K.: Intuitionistic fuzzy sets. In Proceedings of VII ITKR's Session, Sofia, (1983)

[2] Atanassov, K.: Generalized index matrices. Comptes rendus de l'Academie Bulgare des Sciences **40**(11), 15-18 (1987)

[3] Atanassov, K., Szmidt, E. , Kacprzyk, J.: On intuitionistic fuzzy pairs. Notes on Intuitionistic Fuzzy Sets **19**(3), 1-13 (2013)

[4] Atanassov, K., n-Dimensional extended index matrices Part 1. Advanced Studies in Contemporary Mathematics, **28** (2), 245-259 (2018)

[5] Atanassov, K., Marinov, P., Atanassova, V.: InterCriteria analysis with Interval-valued Intuitionistic fuzzy evaluations, in: Cuzzocrea A., Greco S., Larsen H., Saccà D., An-

dreasen T., Christiansen H. (eds) Flexible Query Answering Systems. FQAS 2019, Lecture Notes in Computer Science, Springer, Cham, **11529**, 2019, pp. 329-338

[6] Atanassov, K., Mavrov, D., Atanassova, V.: Intercriteria decision making: a new approach for multicriteria decision making, based on index matrices and intuitionistic fuzzy sets. In: Issues in IFSs and Generalized Nets, vol. 11, pp. 1-8 (2014)

[7] Atanassova V., Doukovska L.: Business Dynamism and Innovation Capability in the European Union Member States in 2018 Through the Prism of InterCriteria Analysis. In: Cuzzocrea A., Greco S., Larsen H., Saccà D., Andreasen T., Christiansen H. (eds) Flexible Query Answering Systems. FQAS 2019. Lecture Notes in Computer Science, **11529** Springer, Cham, 2019, 339-349

[8] Atanassova, V., Roeva, O.: Computational complexity and influence of numerical precision on the results of intercriteria analysis in the decision making process. Notes on Intuitionistic Fuzzy Sets **24**(3), 53-63 (2018) doi: 10.7546/nifs.2018.24.3.53-63

[9] Bureva, V., Sotirova, E., Atanassova, V., Angelova, N., Atanassov, K.: Intercriteria analysis over intuitionistic fuzzy data. In: Lirkov I., Margenov S. (eds) Large-Scale Scientific Computing. LSSC 2017. Lecture Notes in Computer Science, vol. 10665. Springer, Cham, pp. 333-340. Springer, Heidelberg (2018)

[10] Ikonomov, N., Vassilev, P., Roeva, O.: ICrAData - Software for InterCriteria Analysis, Int. Journal Bioautomation **22**(1), 1-10. 2018. doi: 10.7546/ijba.2018.22.1.1-10

[11] Mavrov, D.: Software for InterCriteria Analysis: Implementation of the main algorithm. Notes on Intuitionistic Fuzzy Sets **21**, (2), 2015, 77–86

[12] Traneva, V., Tranev, S., Szmidt, E., Atanassov, K.: Three Dimensional Intercriteria Analysis over Intuitionistic Fuzzy Data. In: Kacprzyk J., Szmidt E., Zadrożny S., Atanassov K., Krawczak M. (eds), IWIFSGN 2017, EUSFLAT 2017. Advances in Intelligent Systems and Computing, vol. 643. Springer, Cham, pp. 442-449 (2017)

[13] Traneva, V., Tranev, S., A multidimensional intuitionistic fuzzy InterCriteria analysis in the restaurant, Journal of intelligent and fuzzy systems, IOS press **Pre-press** (no. Pre-press), pp. 1-18 (2020). doi.org/10.3233/JIFS-189079

[14] Zadeh, L.: Fuzzy Sets. Information and Control 8(3), 338-353 (1965)

[15] InterCriteria Research Portal. http://intercriteria.net/software/. Last accessed 3 december 2020

[16] https://github.com/owid/covid-19-data/tree/master/public/data. Last accessed 5 December 2020

Two-Way Intuitionistic Fuzzy Analysis of Variance for COVID-19 Cases in Europe by Season and Location Factors

Velichka Traneva, Stoyan Tranev

Analysis of variance (ANOVA) is a statistical method concerned with comparing the means of several samples, originally developed by Fisher [5]. When a data set has gaps and irregular changes in consecutive number values (for example, due to varying numbers of tests), this may accumulate a type of uncertainty over multiple reports. Intuitionistic fuzziness provides the means to describe this imprecision more accurrately, by allowing a degree of truth and falsity for a particular statement, where the difference between one and their sum corresponds to the hesitation degree. In previous publications [8, 9, 10, 11], we have introduced one-way (1-D IFANOVA) and two-way (2-D IFANOVA) intuitionistic fuzzy ANOVA , which are based on classical analysis of variance [4], Intuitionistic Fuzzy Sets (IFSs, see [1]) and Index Matrices (IMs, [2]). The pandemic caused by COVID-19 conquered the world in 2020. The recent events related to the COVID-19 pandemic have posed many questions regarding the disease's spread rate, including whether various factors may or may not have an influence upon it.

The present work focuses for the first time on evaluating the spread of COVID-19 in Europe using 2-D IFANOVA approach [9, 10] on the intuitionistic fuzzy dataset of daily cases provided by European Centre for Disease Prevention and Control [13] for the data for the period from March to December 3, 2020. 2-D IFANOVA will establish the impact of "season" and "geographic location" factors for the proliferation of COVID-19 in Europe. The factor "geographic location" of countries involves differing climate, economic development, population density and other properties. The factor "season" involves differing temperature and humidity of the environment. To facilitate the analysis, we have applied the command-line utility "Test2" [10], which performs two-way IFANOVA, over an IM of pre-prepared IFPs. We will also analyse the data with classical ANOVA (which does show a dependency) and will perform a comparative analysis of the results obtained from that and from IFANOVA. The outlined approach for IFANOVA, assisting the decision-making process, can be exended to n-dimensional and can be researched to other types of fuzzy or intuitionistic fuzzy multidimensional data in IMs [3].

Acknowledgements This work is supported by the project of Asen Zlatarov University under Ref. No. NIX-440/2020 "Index matrices as a tool for knowledge extraction".

References

[1] Atanassov, K.: Intuitionistic fuzzy sets. In Proceedings of VII ITKR's Session, Sofia, (1983) (in Bulgarian)

[2] Atanassov, K.: Generalized index matrices. Comptes rendus de l'Academie Bulgare des Sciences **40**(11), 15-18 (1987)

[3] Atanassov, K., n-Dimensional extended index matrices Part 1. Advanced Studies in Contemporary Mathematics, **28** (2), 245-259 (2018)

[4] Doane, D., Seward, L.: Applied statistics in business and economics. McGraw-Hill Education, New York, USA (2016)

[5] Fisher, R.: Statistical Methods for Research Workers, London (1925)

[6] Gil, M.A., Montenegro, M., González-Rodríguez, G., Colubi, A., and Casals, M.R.: Bootstrap Approach to the Multi-sample Test of Means with Imprecise Data, Computer Statistics and Data Analysis, **51**, 148–162 (2006)

[7] Nourbakhsh, M.R., Parchami, A., Mashinchi, M.: Analysis of variance based on fuzzy observations. Int. J. Syst. Sci., **44** (4), 714-726 (2011)

[8] Traneva, V., Tranev, S., Inuitionistic Fuzzy Anova Approach to the Management of Movie Sales Revenue, Studies in Computational Intelligence (2020) (in press)

[9] Traneva V., Tranev S., Inuitionistic fuzzy two-factor analysis of variance of movie ticket sales, Journal of intelligent and fuzzy systems, IOS press (2021) (in press)

[10] Traneva, V., Mavrov, D., Tranev, S.: Intuitionistic Fuzzy Two-Factor Analysis of COVID-19 Cases in Europe, in: Proc. of 2020 IEEE 10th International Conference on Intelligent Systems (IS), Varna, Bulgaria, pp. 533-538 (2020)

[11] Traneva, V., Tranev, S., Inuitionistic Fuzzy Analysis of Variance of Ticket Sales, in: Kahraman, C. (eds.) INFUS 2020, Advances in Intelligent Systems and Computing **1197**, Springer, Cham, 2020, pp. 363–340

[12] Zadeh, L.: Fuzzy Sets. Information and Control 8(3), 338-353 (1965)

[13] www.ecdc.europa.eu/en/publications-data/download-todays-data-geographic-distribution-covid-19-cases-worldwide. Last accessed 25 November 2020

On a Nonlinear Evolution Equation of Magnetic Type Related to a Homogeneous Space

Tihomir Valchev

The main object of study in the present talk is the $1+1$-dimensional nonlinear partial differential equation

$$\mathrm{i}S_t = a[S, S_{xx}] + \frac{3a}{2}\left(S^2 S_x S\right)_x - \left[S^2, S_x\right]_x, \qquad \mathrm{i} = \sqrt{-1}, \qquad a \in \mathbb{C}, \tag{29}$$

that seems to be a novel one. It is assumed that the traceless complex $n \times n$ matrix $S(x,t)$ obeys the additional constraint

$$S^3 = S. \tag{30}$$

In the special case when $S(x,t)$ is an invertible matrix and $a = 2$, (29) turns into the classical Heisenberg ferromagnet equation [1, 3, 5]

$$\mathrm{i}S_t = \frac{1}{2}[S, S_{xx}]. \tag{31}$$

This is why we shall refer to (29) as a generalized Heisenberg ferromagnet equation (GHF). Another interesting special case of (29) is when $a = 0$. Then GHF simplifies to

$$\mathrm{i}S_t + \left[S^2, S_x\right]_x = 0. \tag{32}$$

Such "reduction" is connected to a symmetric space of the series **A.III** and has already been considered in literature, see [2, 4].

Much like the equations (31) and (32), GHF is integrable through inverse scattering transform. Its zero curvature representation is given by the following linear bundle Lax pair in pole gauge

$$\begin{aligned} L(\lambda) &= \mathrm{i}\partial_x - \lambda S, \qquad \lambda \in \mathbb{C}, \\ A(\lambda) &= \mathrm{i}\partial_t + \lambda A_1 + \lambda^2 A_2, \qquad A_2 = \frac{2r}{n} I_n - S^2 + aS, \\ A_1 &= \mathrm{i}a[S, S_x] + \frac{3\mathrm{i}a}{2} S^2 S_x S + \mathrm{i}\left[S_x, S^2\right], \end{aligned} \tag{33}$$

where I_n is the unit matrix of dimension n and $2r$ is the rank of $S(x,t)$. The existence of such representation has deep consequences — it allows one to reduce a complicated nonlinear problem to a linear one that is much easier to study [3, 5]. We shall be particularly interested in the cases when the potential function S is not "generic" but obeys certain extra symmetry condition (reduction), e.g. the pseudo-Hermitian condition

$$\mathcal{E} S^{\dagger}(x,t) \mathcal{E} = S(x,t).$$

Above $\mathcal{E}$ is a diagonal matrix with ± 1 on its principal diagonal and $\dagger$ stands for Hermitian conjugation. Though (29) formally remains the same as a covariant form, the presence of reductions decreases the number of independent entries in $S(x,t)$, i.e. the number of the dynamical fields.

It is well known that Heisenberg ferromagnet equation is gauge equivalent to nonlinear Schrödinger equation [1, 3, 5]. In a quite similar fashion, one can use an appropriate gauge transformation to map (33) to the scattering operator

$$\tilde{L}(\lambda) = \mathrm{i}\partial_x + Q(x,t) - \lambda\Sigma, \qquad \Sigma = \mathrm{diag}\,(I_r, 0, -I_r),$$

where $Q(x,t)$ is some off-diagonal $n \times n$ complex matrix. This "canonical gauge" proves to be very useful when considering direct and inverse scattering problems [3].
Another type of (one-parameter family of) gauge transformations is the so-called dressing transformation. The latter can be effectively applied for one to construct special solutions to (29) in a purely algorithmic way.

References

[1] Fordy A., Kulish P., Nonlinear Schrödinger Equations and Simple Lie Algebras, *Commun. Math. Phys.* **89** (1983) 427–443.

[2] Gerdjikov V., Mikhailov A, Valchev T., Reductions of Integrable Equations on A.III-type Symmetric Spaces, *J. Phys. A: Math. Theor.* **43** (2010) 434015.

[3] Gerdjikov V., Vilasi G, Yanovski A., *Integrable Hamiltonian Hierarchies — Spectral and Geometric Methods*, Springer, Heidelberg, 2008.

[4] Valchev T., Multicomponent Nonlinear Evolution Equations of the Heisenberg Ferromagnet Type. Local Versus Nonlocal Reductions, to appear in Proc. XXII-nd International Conference "Geometry, Integrability and Quantization", June 8–13, 2020, Varna, Bulgaria.

[5] Takhtadjan L., Faddeev L., *The Hamiltonian Approach to Soliton Theory*, Springer, Berlin, 1987.

New Software Functions in Microsoft Excel which can Improve and Facilitate the Work of Internal Auditors when Forming Samples

Veneta Velichkova

The automation of the processes is rapidly and globally increasing as well as the expectations from the auditors to have a deeper knowledge of new technology-based audit techniques to perform their work. Currently, most of the input data which have to be audited subsequently are presented in spreadsheets. Excel is one of the most widespread programs that are used in the industry to process data that is presented in spreadsheets. This program is affordable and in the meantime most appropriate and easy to work with. Using Microsoft Office is an inevitable part of auditing, especially at the stage of Fieldwork, when forming and testing samples.

This research shows how the new dynamic array feature can be used to create random sampling and monetary unit sampling, as they are one of the most commonly used methods of audit sampling. Until now, auditors have been doing this type of work manually which is time-consuming, takes a lot of effort and the risk of error is high. The present study examines how to extract a sample of 30 item records from a data table that contains more than 1000 items records. In the tested columns from the table, we have - number of items, cumulative value, item identifier, and price of the item. For the random type of sampling in the first column, we have to list the number of items we are sampling by using the new function Sequence. In the second column, we create our item sampling by SortBy function that will let us sort our array according to another random array. For this purpose, we use Rand array to generate this random array. Next, we need to pick the chosen number of items for the sample with the Index function and we have the item identifier to the value. Finally, in the third column, we use again Index and Match function to return the price of the selected Items.

In monetary sampling, each currency unit is treated as an element of the population. This sample is applicable when no deviations are expected [1]. In our case, a random dollar of the total amount of dollars should be chosen. First, we use the Sequence function as the number of rows that we are passing as the argument of this function should be the same as the number of the total value. Then we are going to randomise that list using the SortBy function. After that, we convert to find where in the table their possitions are. For this purpose, we Index the Item identifier column and Match this randomly shuffled dollar to the Cumulative value column. The generated data contains duplicates, so we need to use the Unique function. It makes each item to show up only once. The other steps that are performed are the same as random sampling. Again we need to use the Index function and in the next column the Index and the Match to visualise the values.

The results of this study show that for the random sampling the selected items are with smaller values in comparison to the monetary unit sampling because in monetary sampling

larger items are more likely to get picked.

Acknowledgments

I am really grateful to my colleagues at IICT-BAS for the support and all advice they gave me during this research.

References

[1] Veysel, A.: Application of ISA 530 audit sampling, Journal of ICPA, Bulgaria - IDES, 5–18 (2015).

Part B

List of participants

Vera Angelova
Institute of Information and
Communication Technologies
Bulgarian Academy of Sciences
Akad. G. Bonchev, Str., Bl. 2
1113 Sofia, Bulgaria
vangelova@iit.bas.bg

Mikhail Chebakov
Southern Federal University
Bolshaya Sadovaya Str.,
Rostov-on-Don, 344006, Russia
michebakov@yandex.ru

Hristo Chervenkov
National Institute of
Meteorology and Hydrology
Bulgarian Academy of Sciences
Tsarigradsko Shose blvd. 66
1784 Sofia, Bulgaria
hristo.tchervenkov@meteo.bg

Maria Datcheva
Institute of Mechanics
Bulgarian Academy of Sciences
Acad. G. Bonchev Str., Bl. 4
1113 Sofia, Bulgaria
datcheva@imbm.bas.bg

Neli Dimitrova
Institute of Mathematics and Informatics
Bulgarian Academy of Sciences
Acad. G. Bonchev Str., Bl. 8
1113 Sofia, Bulgaria

Ivan Dimov
Institute of Information and
Communication Technologies,
Bulgarian Academy of Sciences
Acad. G. Bonchev Str., bl. 25A
1113 Sofia, Bulgaria
ivdimov@bas.bg

Milena Dimova
University of National and World Economy
Student Town
1700 Sofia, Bulgaria
mkoleva@math.bas.bg

Stefka Fidanova
Institute of Information and
Communication Technologies
Bulgarian Academy of Sciences
Acad. G. Bontchev str., bl. 25A
1113 Sofia, Bulgaria
stefka@parallel.bas.bg

Ivan Georgiev
Institute of Information and
Communication Technologies
Bulgarian Academy of Sciences
Acad. G. Bonchev Str., bl. 2
and
Institute of Mathematics and Informatics
Bulgarian Academy of Sciences
Acad. G. Bonchev str., bl. 8
1113 Sofia, Bulgaria

Krasimir Georgiev
Institute of Mechanics
Bulgarian Academy of Sciences
Acad G. Bonchev Str. Bl. 4
1113 Sofia, Bulgaria

Slavi Georgiev
Angel Kanchev University of Ruse
8 Studentska Str.
7017 Ruse, Bulgaia
georgiev.slavi.94@gmail.com

Stanislav Harizanov
Institute of Information and
Communication Technologies
Bulgarian Academy of Sciences
Acad. G. Bonchev Str., bl. 25A
1113 Sofia, Bulgaria
sharizanov@parallel.bas.bg
and
Institute of Mathematics and Informatics
Bulgarian Academy of Sciences
Acad. G. Bonchev str., bl. 8
1113 Sofia, Bulgaria

R. Hristova
Institute of Information and
Communication Technologies
Bulgarian Academy of Sciences
Akad. G. Bonchev, Str., Bl. 2
1113 Sofia, Bulgaria

Oleg Iliev
Institute of Mathematics and Informatics
Bulgarian Academy of Sciences
Acad. G. Bonchev str., bl. 8
1113 Sofia, Bulgaria
iliev@itwm.fraunhofer.de

Nevena Ilieva
Institute of Information and
Communication Technologies
Bulgarian Academy of Sciences
Acad. G. Bonchev Str, Block 25A
1113 Sofia, Bulgaria
nevena.ilieva@parallel.bas.bg
and
Institute of Mathematics and Informatics
Bulgarian Academy of Sciences
Acad. G. Bonchev str., bl. 8
1113 Sofia, Bulgaria

Tsvetelina I. Ivanova
Institute of Mechanics
Bulgarian Academy of Sciences
Acad G. Bonchev Str. Bl. 4
1113 Sofia, Bulgaria

Juri Kandilarov
Ruse University
8 Studentska Str.
7017 Ruse, Bulgaria
ukandilarov@uni-ruse.bg

Miglena Koleva
Ruse University
6 Studentska St
7017 Ruse, Bulgaria
mkoleva@uni-ruse.bg

Ekaterina Korovaytseva
Institute of Mechanics,
Lomonosov Moscow State University,
Michurinsky prospect 1,
Moscow 119192, Russia
katrell@mail.ru

Elena Kolosova
Southern Federal University
Bolshaya Sadovaya Str.,
Rostov-on-Don, 344006, Russia
a_lena_ch@mail.com

Georgi Kostadinov
Institute of Information and
Communication Technologies
Bulgarian Academy of Sciences
Acad. G. Bonchev Str., Block 25A
1113 Sofia, Bulgaria

Hristo Kostadinov
Institute of Mathematics and Informatics
Bulgarian Academy of Sciences
Acad. G. Bonchev str., bl. 8
1113 Sofia, Bulgaria

Elena Lilkova
Institute of Information and
Communication Technologies
Bulgarian Academy of Sciences
Acad. G. Bonchev Str., Block 25A
1113 Sofia, Bulgaria
elilkova@parallel.bas.bg

Nikolai Manev
Institute of Mathematics and Informatics
Bulgarian Academy of Sciences
Acad. G. Bonchev str., bl. 8
1113 Sofia, Bulgaria

Svetozar Margenov
Institute of Information and
Communication Technologies
Bulgarian Academy of Sciences
Acad. G. Bonchev Str., bl. 25A
1113 Sofia, Bulgaria
margenov@parallel.bas.bg

Geno Nikolov
Sofia University "St. Kliment Ohridski",
Bulgaria
geno@fmi.uni-sofia.bg

Elena V. Nikolova
Institute of Mechanics
Bulgarian Academy of Sciences
Acad. G. Bonchev Str., Bl. 4
1113 Sofia, Bulgaria
elena@imbm.bas.bg

Tzvetan Ostromsky
Institute of Information and
Communication Technologies,
Bulgarian Academy of Sciences
Acad. G. Bonchev Str., bl. 25A
1113 Sofia, Bulgaria
ceco@parallel.bas.bg

Iliyan Petrov
Institute of Information and
Communication Technologies,
Bulgarian Academy of Sciences
Acad. G. Bonchev Str., bl. 2
1113 Sofia, Bulgaria
petrovindex@bas.bg

Kalin Presnakov
Faculty of Mathematics and Informatics
Sofia University "St. Kl. Ohridski"
Blvd. James Bourchier 5
1164 Sofia, Bulgaria
kpresnakov@gmail.com

Sergey Pshenichnov
Institute of Mechanics,
Lomonosov Moscow State University,
Michurinsky prospect 1,
Moscow 119192, Russia
serp56@yandex.ru

Nikolay Shegunov
Faculty of Mathematics and Informatics
Sofia University "St. Kl. Ohridski"
Blvd. James Bourchier 5
1164 Sofia, Bulgaria
nshegunov@fmi.uni-sofia.bg

Dimitar Slavchev
Institute of Information and
Communication Technologies,
Bulgarian Academy of Sciences
Acad. G. Bonchev Str., bl. 25A
1113 Sofia, Bulgaria
dimitargslavchev@parallel.bas.bg

Angela Slavova
Institute of Mathematics and Informatics
Bulgarian Academy of Sciences
Acad. G. Bonchev str., bl. 8
1113 Sofia, Bulgaria

Velislava Stoykova
Institute for Bulgarian Language
Bulgarian Academy of Sciences
1113 Sofia, Bulgaria
vili1@bas.bg

Michail D. Todorov
Technical University of Sofia
Sofia, Bulgaria
mtod@tu-sofia.bg

Venelin Todorov
Institute of Information and
Communication Technologies
Bulgarian Academy of Sciences
Acad. G. Bonchev Str., bl. 25A
1113 Sofia, Bulgaria
dvespas@mail.bg

Petar Tomov
Institute of Information and
Communication Technologies
Bulgarian Academy of Sciences
Acad. G. Bonchev Str., Block 2
1113 Sofia, Bulgaria

Stoyan Tranev
"Prof. Asen Zlatarov" University
"Prof. Yakimov" Blvd 1
8000 Burgas, Bulgaria

Velichka Traneva
"Prof. Asen Zlatarov" University
"Prof. Yakimov" Blvd 1
8000 Burgas, Bulgaria

Tihomir Valchev
Institute of Mathematics and Informatics
Bulgarian Academy of Sciences
Acad. Georgi Bonchev Str., Block 8
1113 Sofia, Bulgaria

Veneta Velichkova
Institute of Information and
Communication Technologies
Bulgarian Academy of Sciences
Acad. G. Bonchev Str., Block 25A
1113 Sofia, Bulgaria

Nikolay K. Vitanov
Institute of Mechanics
Bulgarian Academy of Sciences,
Acad. G. Bonchev Str.,Bl. 4
1113 Sofia, Bulgaria
vitanov@imbm.bas.bg

Lubin Vulkov
Ruse University
6 Studentska St
7017 Ruse, Bulgaria
lvalkov@uni-ruse.bg

Iliyan Zankinski
Institute of Information and
Communication Technologies
Bulgarian Academy of Sciences
Acad. G. Bonchev Str., Block 25A
1113 Sofia, Bulgaria

Plamena Zlateva
Institute of Mathematics and Informatics
Bulgarian Academy of Sciences
Acad. G. Bonchev Str., Bl. 8
1113 Sofia, Bulgaria